

# Passive receptor dissociation driven by porin threading establishes active colicin transport through *Escherichia coli* OmpF

Marie-Louise R. Francis<sup>1†‡</sup>, Melissa N. Webby<sup>1†</sup>, Nicholas G. Housden<sup>1</sup>, Renata Kaminska<sup>1</sup>, Emma Elliston<sup>1¶</sup>, Boonyaporn Chinthammit<sup>1§</sup>, Natalya Lukoyanova<sup>2</sup> and Colin Kleanthous<sup>1\*</sup>

<sup>†</sup>Authors contributed equally to this work

<sup>1</sup>Department of Biochemistry, South Parks Road, University of Oxford, Oxford OX1 3QU, UK

<sup>2</sup>Department of Biological Sciences, ISMB, Birkbeck College, London WC1E 7HX, UK

<sup>‡</sup>Present address: NovaBiotics, Unit 3 Silverburn Crescent, Bridge of Don, Aberdeen AB23 8EW, UK

<sup>§</sup>Present address: University College London, Gower Street, London WC1E 6BT, UK

<sup>¶</sup>Present address: Arnold & Porter Kaye Scholer LLP, Tower 42, 25 Old Broad Street, London, EC2N 1HQ, UK

\*Address for Correspondence: Professor Colin Kleanthous, Department of Biochemistry, South Parks Road, University of Oxford, Oxford OX1 3QU, UK. Email: colin.kleanthous@bioch.ox.ac.uk. Tel: +44-1865-613370

## 26 SUMMARY

27 Bacteria deploy weapons to kill their neighbours during competition for resources and aid  
 28 survival within microbiomes. Colicins were the first antibacterial system identified yet how  
 29 these bacteriocins cross the outer membrane of *Escherichia coli* is unknown. Here, by  
 30 solving the structures of translocation intermediates and imaging toxin import, we uncover  
 31 the mechanism by which the Tol-dependent nuclease colicin E9 (ColE9) crosses the outer  
 32 membrane. We show that threading of ColE9's disordered domain through two pores of the  
 33 trimeric porin OmpF causes the colicin to disengage from its primary receptor, BtuB, and  
 34 reorganise the translocon either side of the membrane. These rearrangements prime the  
 35 toxin for import through the lumen of a single OmpF subunit, which is driven by the proton  
 36 motive force-linked TolQ-TolR-TolA-TolB assembly. Our study explains why OmpF is a  
 37 better translocator than OmpC and reconciles the mechanisms by which Ton- and Tol-  
 38 dependent bacteriocins cross the bacterial outer membrane.

39

40 Word count, 150

41

## 42 Introduction

43 The asymmetric outer membrane (OM) of Gram-negative bacteria, composed of  
 44 lipopolysaccharides (LPS) in the outer leaflet and phospholipids in the inner leaflet, shields  
 45 the organism against environmental insults, the immune systems of plants and animals, bile  
 46 salts in the human gut and several classes of antibiotics (Nikaido, 2003; Ranf, 2016; Vergalli  
 47 et al., 2020; Whitfield and Trent, 2014). Bacteria have nevertheless evolved potent  
 48 antibacterial systems to breach the OM that are integral to the internecine warfare between  
 49 bacterial populations as they compete for space in which to grow and nutrients on which to  
 50 feed (Granato et al., 2019). Attack strategies are typically of two types, those that depend  
 51 on physical or close contact between bacterial cells and those mediated by diffusible  
 52 molecules (Ruhe et al., 2020). The former includes contact-dependent inhibitors, where a  
 53 toxin projected from an attacking cell binds a surface receptor of a recipient cell prior to  
 54 import (Aoki et al., 2010), and type VI secretion, where toxins are delivered by a needle that  
 55 punctures the OM (Basler et al., 2013). Diffusible toxins are generally referred to as  
 56 bacteriocins and can be peptides or proteins. Here, we focus on a family of protein  
 57 bacteriocins from the antimicrobial armoury of the *Enterobacteriaceae* and reveal their  
 58 convoluted use of porins for OM transport.

59 Protein bacteriocins (hereafter referred to as bacteriocins) are plasmid or  
 60 chromosomally-encoded multidomain toxins that kill cells through the action of a C-terminal  
 61 cytotoxic domain orchestrated by N-terminal regions of the toxin (Kleanthous, 2010).  
 62 Cytotoxic activity is expressed either in the periplasm, through depolarisation of the  
 63 cytoplasmic membrane or cleavage of the lipid II peptidoglycan precursor, or in the  
 64 cytoplasm through cleavage of specific tRNAs, ribosomal RNA or chromosomal DNA.  
 65 Passage across the OM is catalysed by one of two proton-motive force (PMF)-linked  
 66 assemblies in the inner membrane. Ton-dependent (group B) bacteriocins contact TonB  
 67 via TonB-dependent transporters (TBDTs) in the OM whereas Tol-dependent (group A)

bacteriocins contact one or more components of the Tol-Pal system (Cascales et al., 2007). Nearly all Tol-dependent bacteriocins identified to-date enter bacteria using a porin in combination with an outer membrane protein receptor, which can be a neighbouring TBDT or the porin itself (Kleanthous, 2010). *E. coli* porins OmpF and OmpC are abundant trimeric  $\beta$ -barrel outer membrane proteins with narrow channels running through them that taper to an eyelet, 7-8 Å at the narrowest point (Nikaido, 2003). The dimensions and electrostatic nature of the eyelet allow the diffusion of nutrients and metabolites (<600 Da) but excludes large antibiotics such as vancomycin and folded proteins.

Recent work has shown that Ton-dependent bacteriocins specific for *Pseudomonas aeruginosa* are transported unfolded through TBDTs (White et al., 2017). Import is energized by the PMF via TonB and its associated ExbB-ExbD stator complex. By contrast, controversy surrounds how Tol-dependent bacteriocins exploit porins to cross the OM and whether this transport is energized. The present work focuses on the group A endonuclease (DNase) colicin, ColE9, a member of the E group of colicins (ColE2-E9), all of which use the same import machinery but target different nucleic acids in the cytoplasm (DNA, rRNA or tRNAs) (Kleanthous, 2010). We demonstrate using cryo-EM and live-cell imaging that ColE9 exploits the trimeric porin OmpF to cross the OM of *E. coli* by a combination of passive and active transport. We show that following binding to its TBDT receptor, BtuB, ColE9 threads its disordered N-terminus through two subunits of OmpF both as a means of capturing a component of the PMF-coupled Tol-Pal system in the periplasm but also to disengage the toxin from its receptor. ColE9 then translocates unfolded through the narrow lumen of a single OmpF subunit by a process that is entirely driven by the PMF. We also demonstrate that large fluorophores normally excluded by the pores of OmpF can be forcibly brought into the cell by attaching them to the colicin.

92

93

## Results

### *Cryo-EM structure of the ColE9 outer membrane translocon*

ColE9 is a plasmid-encoded heterodimer comprising a 60-kDa toxin bound to a small immunity protein, Im9. The two proteins are released together from *E. coli* cells in response to environmental stress (Cooper and James, 1984). Immunity proteins are high-affinity inhibitors that are co-expressed with the colicin and protect the producing cell from its cytotoxic action (Kleanthous et al., 1999), but are jettisoned during import of the bacteriocin (Vankemmelbeke et al., 2013). ColE9 has four functionally annotated domains (**Figure 1a**) (Klein et al., 2016). At the N-terminus, an 83 amino acid intrinsically-unstructured translocation domain (IUTD) houses three protein-protein interaction epitopes (Housden et al., 2010); a 16-residue TolB-binding epitope (TBE) associates with the periplasmic protein TolB and this is flanked by two OmpF-binding sites (OBS1 and OBS2). The IUTD is followed by a folded  $\alpha/\beta$  domain which is thought to be associated with inner membrane translocation and generally referred to as the translocation or T-domain. Following the T-domain is a long coiled-coil receptor-binding (R-) domain the apex of which binds the vitamin B<sub>12</sub> transporter BtuB on the cell surface (**Figure 1b**). Finally, at the C-terminus of the colicin is a cytotoxic DNase to which the immunity protein Im9 is bound. Following import and ejection of Im9, the internalised DNase elicits cell-death through random cleavages of the bacterial genome. The ColE9 DNase is a member of the H-N-H/ $\beta\beta\alpha$ -Me class of metal-dependent endonucleases (Pommer et al., 2001), which includes apoptotic nucleases and the core nuclease of CRISPR/Cas9. Other cytotoxic domains can be delivered by the same toxin chassis, including the RNase of ColE3 that inhibits protein synthesis by site-specific cleavage of the ribosomal A-site (Ng et al., 2010). The structures of ColE3 (Soelaiman et al., 2001) and ColE9 (Klein et al., 2016) have been reported previously as have the binary

119 complexes of ColE3 R-domain-BtuB (Kurusu et al., 2003), ColE9 OBS1-OmpF (Housden et  
120 al., 2010) and ColE9 TBE-TolB (Loftus et al., 2006).

121 Tol-dependent colicins assemble a translocon at the cell surface that involves its  
122 periplasmic target along with the OM receptor and translocator which together establish the  
123 import pathway of the toxin. No structures have yet been reported for any colicin translocon  
124 and so there is little understanding of how these assemblies underpin OM transport. We  
125 have reported previously the isolation and purification of the entire OM translocon for ColE9  
126 in which the toxin, bound to TolB, BtuB, and OmpF, is solubilised in 1%  $\beta$ -octylglucoside ( $\beta$ -  
127 OG) (Housden et al., 2013). This complex is in addition stabilised by a disulphide bond at  
128 the periphery of the ColE9 TBE-TolB interface which does not impact the protein-protein  
129 interface (Housden et al., 2013). We followed the same procedure, which involves a  
130 combination of *in vivo* and *in vitro* approaches, but, for ease of assembly (see Materials and  
131 Methods), using ColE9 truncated at the end of the R-domain and hence missing both the  
132 DNase and Im9. The assembled translocon was transferred into amphipols and vitrified on  
133 graphene oxide coated grids for visualisation of individual particles by cryo-EM (see  
134 Materials & Methods for details).

135 Single particle analysis revealed the presence of two populations of ColE9 translocon  
136 complexes, one where the translocon was intact and a second class where BtuB was absent,  
137 which we refer to as the partial translocon (**Supplementary Figures 1 and 2**). The final  
138 post-processed map of the full translocon (**Figures 1c and d**) is at an overall resolution of  
139 4.7 Å, according to the gold-standard FSC method, with local resolutions ranging from 4.7  
140 to 16 Å. The absence of BtuB in the partial translocon resulted in an improvement in map  
141 resolution (**Figures 1e and f**), which varies from 3.7 to 6 Å (FSC). Masked subtraction of  
142 BtuB from the full translocon map and refinement of these subtracted particles did not  
143 improve map quality, suggesting that it is the loss of BtuB from the complex which resulted  
144 in the increase in map resolution. Density for ColE9 was better resolved in the full compared

to the partial translocon where only the T-domain was resolved. This is most likely due to the ColE9 R-domain providing some conformational rigidity in the fully assembled translocon through its interaction with BtuB. This contention is supported by the loss of density for the R-domain in the partial translocon map. By contrast, density for TolB was better resolved in the partial translocon map. The partial translocon map presented here is similar to a negative stain map of a proteolysed version of the translocon (comprising of OmpF, TolB and ColE9 residues 1-122), reported previously at a resolution  $\sim 20$  Å ((Housden et al., 2013). However, the lower resolution of this earlier structure meant little information was forthcoming about ColE9 interactions with OmpF.

Isolated crystallographic structures for the majority of ColE9 translocon components provided a starting point for model building into the full and partial translocon maps. Although the resolution of the full translocon map did not allow for local refinement of docked structures, rigid-body refinement was carried out to generate a molecular model. For the partial translocon model, OmpF was docked and refined locally along with the ColE9 IUTD (residues 3-75), which were built *de novo* into the map. The remaining ColE9 T-domain residues (85-316) and TolB were rigid-body refined into the partial translocon map due to the lower resolution associated with these parts of the map.

In the fully assembled translocon model, the 22-stranded  $\beta$ -barrel of BtuB sits at a  $35^\circ$  angle relative to the trimeric  $\beta$ -barrel structure of OmpF (**Figures 1c and d**). Unmodelled density, most likely that of a single molecule of LPS, is wedged between the two proteins which likely contributes to displacement of BtuB relative to OmpF. Native state mass spectrometry has shown previously that a single LPS molecule remains associated with the purified translocon complex (Housden et al., 2013). Since there are no examples in the PDB of heterologous bacterial outer membrane proteins residing next to each other it is not clear if the  $35^\circ$  tilt reflects the natural position of BtuB in the OM or the way in which the ColE9 translocon was assembled for cryo-EM analysis. We note however that if the  $\beta$ -

171 barrels of OmpF and BtuB were flush in the membrane the 45° trajectory of the ColE9 R-  
 172 domain-BtuB complex, first shown for the ColE3 R-domain-BtuB complex (0.95 Å rmsd)  
 173 (Kurusu et al., 2003), would project the T-domain beyond OmpF. The coiled-coil nature of  
 174 the R-domain, with BtuB at its apex, means the cytotoxic DNase domain although absent  
 175 from the current structure would sit ~60 Å above OmpF. Finally, TolB is held on the  
 176 periplasmic side of OmpF through its association with the ColE9 TBE, but is not well-  
 177 resolved in the full translocon model (**Figures 1c and d**).

178 The partial translocon is comprised of OmpF, the IUTD and T-domain of ColE9 and  
 179 TolB (**Figures 1e and f**). Previous work on the translocation mechanism of group A colicins  
 180 has demonstrated that these colicins contact their periplasmic binding partners (typically  
 181 TolB and/or TolA) by a direct epitope delivery mechanism following binding to the cell  
 182 surface receptor (Housden et al., 2010; Jansen et al., 2020). The colicin threads its IUTD  
 183 through two of OmpF's three pores thereby presenting a tethered protein-protein interaction  
 184 epitope to the periplasm. In the case of ColE9, the TBE promotes contact between TolB  
 185 and TolA in the inner membrane which is coupled to the PMF through its partners, TolQ and  
 186 TolR (Bonsor et al., 2009). The partial translocon structure of ColE9 shows how the IUTD  
 187 (residues 3-75) navigates through the lumen of one OmpF subunit in order to thread back  
 188 up into a neighbouring subunit. The end result is that each OBS is lodged within an  
 189 individual subunit of OmpF: OBS1 (residues 2-18) is bound to subunit 1 while OBS2  
 190 (residues 54-63) is bound to subunit 2, leaving subunit 3 free of colicin. The relative  
 191 positions of the two OBSs in the partial translocon model implies that subunit 2 is the entry  
 192 port for the ColE9 IUTD following its initial binding to BtuB in the OM.

193 The resolution of the full translocon does not allow for detailed comparison of OBS  
 194 binding with that of the partial translocon (details below), however an overlay of the two  
 195 models reveal that the ColE9 T-domain undergoes a large-scale movement, rotating by 15°  
 196 and moving vertically by 12 Å along the rotation axis (**Figures 2a-c**). In the full translocon,

the orientation of the ColE9 T-domain is fixed by the R-domain's contact with BtuB. Rotation of the ColE9 T-domain in the partial translocon to achieve the orientation adopted in the full translocon structure results in a poorer fit to map density. Importantly, rotation of the ColE9 T-domain from the full to the partial translocon repositions ColE9 from a central position above the OmpF trimer to become localised above subunit 2 within which OBS2 is bound (**Figures 3a and c**).

TolB also undergoes large-scale movements when transitioning from the full to partial translocon structures, which are likely linked to the re-arrangement of the ColE9 T-domain on the extracellular side of the porin (**Figures 2d and e**). The position of TolB is rotated by  $\sim 50^\circ$  between the two structures and in the partial translocon is located closer to OmpF through a  $\sim 8$  Å upward movement along the axis of rotation. The positioning of TolB closer to OmpF in the partial translocon structure is stabilised by additional interactions between the periplasmic region of OmpF subunit 1 and the IUTD sequence immediately preceding the TBE (**Figure 3g**). Irrespective of the observed movements between the two Cryo-EM models, TolB remains located beneath subunit 2 within which OBS2 is bound.

In summary, we have solved the first cryo-EM structure of a colicin OM translocon. The structure of ColE9 is associated with its full complement of OMP translocation components, BtuB and OmpF, as well as its periplasmic target TolB. We have also solved a partial translocon structure in which the primary receptor BtuB is missing, which leads to substantial rearrangements of ColE9 and TolB above and below the membrane, respectively. As we demonstrate below, these structural changes within the translocon complex are integral to the mechanism by which ColE9 translocates across the OM.

#### *ColE9 IUTD interactions with the subunits of OmpF*

The higher resolution structure of the partial ColE9 translocon provides a molecular explanation as to how bacteriocins exploit porins to establish their translocon complexes at

223 the OM. The lumen of an OmpF monomer is not a straight channel but akin to an hour-  
 224 glass (**Figures 3a-c**). The outer (extracellular side) and inner (periplasmic side) vestibules  
 225 of OmpF have diameters of 25 Å and 30 Å, respectively, constricting at the eyelet of the  
 226 channel to ~7 Å. After the IUTD region passes through OmpF subunit 2, OBS1 threads  
 227 back up into subunit 1 such that it snakes along the bottom of the lumen at its widest point  
 228 and finishes up at the eyelet (**Figures 3a and b**). By contrast, OBS2 spans the eyelet of  
 229 OmpF subunit 2 via a kink created at Gly61, which is enforced by the hydrogen bonding of  
 230 neighbouring residues, Ser60 and Arg62 (**Figure 3c**). After OBS2 traverses the eyelet, the  
 231 remaining ColE9 sequence does not track the OmpF interior as observed for OBS1, instead  
 232 remaining more centrally located in the inner vestibule.

233 The bound conformations of the two OBSs are stabilised by electrostatic and  
 234 hydrogen bonding interactions (**Figures 3d-h**). The vestibules and eyelet of OmpF are  
 235 highly charged environments; the porin exhibits slight cation selectivity in solute diffusion  
 236 studies (Basle et al., 2006). Charged patches within the eyelet of OmpF are matched by  
 237 opposing charges of the OBS sequences (**Figures 3d and e**). In addition to these  
 238 interactions, networks of hydrogen-bonds lock OBS1 and OBS2 of ColE9 into defined  
 239 conformations within their respective OmpF subunits (**Figures 3f and h**). Key OBS1  
 240 residues that interact with subunit 1 include Asp5, Arg7, Thr11, Ser15, and Ser17 (**Figures**  
 241 **3f and g**). Previous studies have shown that mutation of Asp5, Arg7 or Thr11 to alanine  
 242 substantially weakens OmpF binding by OBS1 while an Asp5Ala/Arg7Ala double mutant  
 243 abolishes OmpF binding, consistent with their essential role in stabilising the OBS1-OmpF  
 244 subunit 1 complex (Housden et al., 2005; Housden et al., 2010). We have reported  
 245 previously the 3 Å crystal structure of an OBS1 peptide bound to OmpF (Housden et al.,  
 246 2010). At the time, there was uncertainty as to the orientation of the peptide, which was  
 247 refined with the N-terminus facing the periplasm. We re-processed these data and rebuilt  
 248 the model based on the orientation observed in the cryo-EM data for the partial translocon,

249 validating this re-processed model (**Supplementary figures 2k-m**). The new model shows  
 250 conclusively that OBS1 has its N-terminus pointing towards the extracellular environment  
 251 (**Figure 3a**) and in both models the conformation adopted by OBS1 is identical. This  
 252 orientation agrees with recent electrophysiological data and live-cell imaging experiments  
 253 all of which show OBS1 binding subunit 1 of OmpF from the periplasm (Housden et al., 2018;  
 254 Lee et al., 2020). In contrast to OBS1, the hydrogen bond network that stabilises OBS2  
 255 within subunit 2 of OmpF primarily involves OBS2 backbone atoms and OmpF side-chains  
 256 (**Figure 3h**), likely explained by the high glycine content within the OBS2 sequence (6/11  
 257 residues are glycine, compared to 6/16 for OBS1). The high glycine content also explains  
 258 how OBS2 can bind in an extended conformation to OmpF, traversing the narrow eyelet.  
 259 Only two OBS2 residues, Trp56 and Arg62, form side-chain hydrogen bonds with OmpF.

260 In conclusion, the bound conformations of the OBS epitopes within the electrostatic  
 261 pores of OmpF are stabilised by salt bridges, backbone and sidechain hydrogen bonds and  
 262 aided by their high glycine content. The specific binding modes of each OBS is explained  
 263 by their specific set of interactions within identical OmpF pores and, in the case of OBS1,  
 264 through directional insertion into the binding site from the periplasm.

265

266 *Threading ColE9's IUTD through the pores of OmpF passively displaces the toxin from its*  
 267 *primary receptor, BtuB*

268 The structural differences evident between the full and partial ColE9 translocons  
 269 centre around the loss of BtuB from the complex. Concomitant with this loss is the  
 270 restructuring of the ColE9 T-domain and TolB so that, linked by the OBS2 epitope, the two  
 271 proteins become positioned immediately above and below, respectively, subunit 2 of OmpF.  
 272 Given the precise nature of these rearrangements we hypothesised that the partial  
 273 translocon may be indicative of an intermediate state subsequent to ColE9 docking onto the  
 274 cell surface. To test this hypothesis, we exploited the observation that the isolated R-domain

275 of ColE9 inhibits the growth of an *E. coli* strain dependent on vitamin B<sub>12</sub> (**Figure 4a**)  
 276 (Penfold et al., 2000). *E. coli* 113/3 is a *metE* mutant that requires vitamin B<sub>12</sub> to synthesise  
 277 methionine. Since the 76-residue ColE9 R-domain competitively blocks binding of vitamin  
 278 B<sub>12</sub> to BtuB and binds with higher affinity its addition to *E. coli* 113/3 grown in minimal media  
 279 supplemented with vitamin B<sub>12</sub> suppresses cell growth. We repeated this experiment using  
 280 an identical concentration of intact ColE9 harbouring a single mutation, W39A, within its  
 281 TBE. Substitution of ColE9 Trp39 for alanine inactivates the toxin by abolishing binding to  
 282 TolB in the periplasm, which in turn disengages the colicin from the PMF-coupled TolQ-  
 283 TolR-TolA complex in the IM (Hands et al., 2005). Hence, while all other OM interactions of  
 284 the colicin are those of the wild-type toxin, ColE9 W39A cannot deliver its DNase into the  
 285 cell. Addition of ColE9 W39A to *E. coli* 113/3 largely restored cell growth under conditions  
 286 where the isolated R-domain inhibited growth (**Figure 4a-c**). These data imply, along with  
 287 the cryo-EM data, that subsequent to binding BtuB in the OM, threading of the ColE9 IUTD  
 288 through two subunits of OmpF to form the translocon results in the toxin disengaging from  
 289 BtuB. This translocon-induced dissociation is a passive process since ColE9 W39A is  
 290 unable to engage with the energised Tol-Pal system. We next investigated if and when the  
 291 PMF is engaged in OM transport of the colicin.

292

### 293 *The electrical potential of the PMF drives ColE9 import across the OM*

294 Assembly of ColE9's OM translocon occurs without the input of cellular energy,  
 295 including dissociation from the BtuB receptor. At this point in the import process ColE9 is  
 296 composed of multiple folded domains so this raised the question of whether transport across  
 297 the OM involved the PMF in order that domain unfolding could occur. Earlier studies  
 298 suggested some form of unfolding to be involved; inferred from the activating effects of urea  
 299 on colicin toxicity and the inhibitory effects of intramolecular disulphide bonds (Benedetti et  
 300 al., 1992; Housden et al., 2005). However, the involvement of the PMF in Tol-dependent

301 nuclease colicin entry is controversial. A recent model, for example, suggests that instead  
302 of energised transport, passive, electrostatically-driven ratcheting of the colicin nuclease  
303 occurs through the one remaining unoccupied subunit of OmpF (subunit 3 in the present  
304 work) once the translocon is formed (Cramer et al., 2018).

305 A major issue the bacteriocin field has faced thus far in establishing if transport across  
306 the OM is energised is the lack of appropriate measures of transport that are not dependent  
307 on cell death as a readout. To address this problem, we developed a live-cell imaging  
308 platform using fluorescently-labelled ColE9. A single cysteine mutation was engineered at  
309 Lys469 in the ColE9 DNase domain (**Figure 1b**), which would be the last domain of the  
310 colicin to enter if the toxin was pulled into the cell by the Tol-Pal system. Lysine 469 is  
311 adjacent to the DNase active site (**Supplementary figure 3a**). The mutant was labelled  
312 initially with AlexaFluor (AF) 647 and excess dye removed by gel-filtration chromatography.  
313 Labelling efficiency was typically 90-100% for this and all other fluorophores used in this  
314 study (see Materials and Methods for details). The impact of labelling ColE9 K469C on  
315 biological activity was assessed by a plate-killing assay, where serial dilutions of the colicin  
316 were pipetted onto a lawn of susceptible *E. coli* JM83 cells and grown overnight  
317 (**Supplementary figure 4**). Wild-type ColE9 typically shows killing activity against *E. coli*  
318 JM83 (a K-12 strain) down to ~50 pM. Labelling ColE9 K469C with AF647 reduced colicin  
319 activity by ~two-orders of magnitude relative to wild-type ColE9, which nevertheless  
320 represents significant toxicity since clearance zones are visible at low nanomolar  
321 concentrations. The decrease in activity could be the result of the fluorophore affecting  
322 cytotoxicity and/or import. Alternatively, if labelling completely abolished colicin activity the  
323 residual toxicity might simply reflect the presence of unlabelled molecules.

324 In order to distinguish between these possibilities, we investigated the effect of  
325 labelling the same position with fluorophores of differing size and charge (AF488, AF568,  
326 AF647). We rationalized that if decreased colicin activity reflected unlabelled molecules

327 then altering the fluorophore would have a negligible effect given that the maleimide  
 328 chemistry used to attach the fluorophores was the same in each case. None of the  
 329 fluorophores attached at this position affected the ability of the isolated nuclease domain of  
 330 ColE9 to degrade dsDNA (**Supplementary figure 3b-e**). We next repeated the *E. coli* JM83  
 331 cell-killing assay for the ColE9 K469C mutant labelled with each of the fluorophores. These  
 332 experiments showed that the fluorophores affected toxicity to varying degrees; the order of  
 333 their impact being AF568>AF647>AF488 (**Supplementary figure 4**). Indeed, ColE9  
 334 K469C<sup>AF568</sup> displayed very little colicin activity. Finally, we conducted further *in vivo* tests by  
 335 assessing the impact of fluorophore labelling ColE9 K469C on the activation of the DNA  
 336 damage-induced SOS response in *E. coli* cells (**Supplementary figure 5a-d**). Transported  
 337 ColE9 readily activates SOS through cleavage of chromosomal DNA, which can be  
 338 monitored by *lux* bioluminescence in an *E. coli* reporter strain (DPD1718) (see Materials and  
 339 Methods). As reported previously (Vankemmelbeke et al., 2005), ColE9 above 20 nM  
 340 completely arrested growth of DPD1718 in liquid culture at 37 °C after 90 min and this  
 341 corresponded to a peak in *lux* bioluminescence, which then subsided to zero as all cells  
 342 were killed-off (**Supplementary figure 5b**). Lower concentrations of ColE9 resulted in the  
 343 same initial increase in *lux* bioluminescence but did not subside because cell growth begins  
 344 to outcompete colicin toxicity. While none of the fluorophore labelled ColE9 constructs (at  
 345 20 nM) significantly impacted growth of *E. coli* DPD1718, all resulted in *lux* bioluminescence  
 346 albeit with altered kinetics (**Supplementary figure 5c and d**). The suppression of signal  
 347 observed in these experiments mirrored their impact in the cell-killing plate assays  
 348 (**Supplementary figure 4**). Combined, these experiments imply that fluorophore labelling  
 349 of ColE9 K469C affects the kinetics of colicin-mediated killing and that the identity of the  
 350 fluorophore is a significant factor. The molecular basis of this effect is explored further below.  
 351 We conclude that the residual toxicity of fluorescently-labelled ColE9 reflects a reduced  
 352 capacity to transport into *E. coli* rather than the activity of unlabelled molecules.

353 Since fluorescently labelled ColE9 can be imported into *E. coli* we exploited this  
354 approach to probe the PMF dependence of import using fluorescence microscopy. For  
355 these experiments, ColE9 K469C<sup>AF647</sup> was used because it circumvented cell auto-  
356 fluorescence issues associated with using AF488 and had lower impact on colicin-mediated  
357 killing than AF568. An active site mutation (H551A hereafter denoted as \*; **Supplementary**  
358 **figure 3a**) was also introduced in the ColE9 K469C background to avoid killing cells during  
359 long time-courses. Following the labelling of cellular DNA with Hoechst stain, ColE9\*  
360 K469C<sup>AF647</sup> was added to *E. coli* JM83 cultures, the excess fluorophore removed by  
361 repeated wash steps and cells imaged on agar pads by widefield fluorescence microscopy  
362 (see Materials and Methods for details). In contrast to whole cell labelling by Hoechst,  
363 ColE9\* K469C<sup>AF647</sup> predominantly labelled the cell periphery (**Figure 5a and b**). To ensure  
364 labelling was specific for the ColE9 receptor BtuB, the experiment was repeated using a  
365 *btuB* deletion mutant, which abolished labelling by ColE9\* K469C<sup>AF647</sup> (**Figure 5c**). To  
366 determine if ColE9\* K469C<sup>AF647</sup> was surface exposed, labelled cells were treated with  
367 trypsin prior to imaging. Following this treatment, significant fluorescence remained  
368 associated with the cells suggesting these were imported molecules protected from  
369 proteolysis (**Figure 5a-c**). When cells were pre-treated with the protonophore CCCP, all  
370 ColE9\* K469C<sup>AF647</sup> fluorescence was lost from cells when trypsin was added (**Figure 5a-c**),  
371 with similar results observed for cells labelled with ColE9\* K469C carrying AF488 or AF568  
372 fluorophores (**Supplementary figure 6a and b**). Consistent with a role for PMF in ColE9\*  
373 K469C<sup>AF647</sup> import, pre-treatment of cells with ColB, a Ton-dependent pore-forming colicin  
374 that depolarises the inner membrane, also blocked uptake of ColE9\* K469C<sup>AF647</sup> across the  
375 OM similar to the effects of CCCP (**Supplementary figure 6c and d**). As a final test for the  
376 involvement of the PMF in ColE9\* K469C<sup>AF647</sup> import, nigericin and valinomycin, which  
377 inhibit the proton gradient ( $\Delta\text{pH}$ ) and electrical potential ( $\Delta\Psi$ ) components, respectively,  
378 were added to cells prior to labelling (**Supplementary figure 7**). Of these, only valinomycin

379 blocked the uptake of the colicin from which it can be inferred that it is the electrical potential  
380 of the PMF that drives ColE9 translocation across the OM. We conclude that while formation  
381 of the OM translocon complex at the cell surface is passive, import of ColE9 across the  
382 membrane is an energised process that requires the electrical potential of the PMF.

383  
384 *ColE9 translocates through the pore of a single OmpF subunit*

385 The structural changes evident within the ColE9 translocon on displacement of BtuB,  
386 whereby the T-domain becomes repositioned immediately above the same OmpF subunit  
387 (subunit 2) as TolB in the periplasm, are consistent with OmpF being the port of entry.  
388 Indeed, OmpF eyelet mutations are known to confer resistance to Tol-dependent colicins  
389 (Jeanteur et al., 1994). The absolute requirement for the electrical potential of the PMF to  
390 import ColE9 across the OM further supports this contention since this could provide the  
391 cellular energy needed to unfold the toxin for passage through the porin. We hypothesised  
392 that if ColE9 passes directly through the eyelet then the physicochemical properties of both  
393 the colicin and the eyelet would be important factors in transport. A clue that this might be  
394 the case came from the experiments showing that three fluorophores (AF488, AF568,  
395 AF647) differentially affected the ability of ColE9 to induce the SOS response in *E. coli*  
396 DPD1718 cells (**Supplementary figure 5**); the fluorophores have molecular weights (720-  
397 1250 Da) significantly greater than are permissive in porin solute diffusion assays (Vergalli  
398 et al., 2020) yet did not impact colicin activity similarly. A complicating factor in interpreting  
399 these experiments however is the presence of both OmpF and OmpC in the OM of typical  
400 *E. coli* K-12 strains, the ratios of which change depending on the osmolarity, pH and  
401 temperature of the growth medium (Pratt et al., 1996). The two porins share 60% sequence  
402 identity, have similar trimer structures and eyelet dimensions and can form mixed trimers in  
403 the OM (Gehring and Nikaido, 1989). Where they differ however is the degree of negative  
404 charge at the eyelet; OmpC is significantly more electronegative than OmpF (**Figure 6a**).

405 We therefore assessed the impact of fluorophore labelling on the ability of ColE9 K469C to  
 406 kill *E. coli* strains expressing either OmpF or OmpC in the OM. Wild-type, unlabelled ColE9  
 407 killed both strains equally well in plate-killing assays (**Figure 6b**). Fluorophore labelling had  
 408 a modest impact on OmpF-expressing cells whereas cytotoxicity was largely abolished in  
 409 OmpC-expressing cells (**Figure 6b**), especially for AF568 and AF647-labelled ColE9.  
 410 These fluorophores carry -2 and -3 charges, respectively, and are the largest of the three  
 411 fluorophores used (880 and 1250 Da, respectively, compared to 720 Da for AF488). Lastly,  
 412 we investigated the ability of AF647-labelled ColE9 to translocate into *ompF*- or *ompC*-  
 413 expressing cells using wide-field fluorescence microscopy with or without trypsin treatment.  
 414 Here again, the presence of the fluorophore had a much greater impact on the ability of the  
 415 colicin to enter *ompC*-expressing cells compared to those expressing *ompF* (**Figure 6c and**  
 416 **d**). We conclude that the slightly narrower pore and greater negative charge of the OmpC  
 417 eyelet act as significant impediments to ColE9 import when the colicin has a large (>600  
 418 Da), negatively charged fluorophore covalently attached to its C-terminal DNase domain, an  
 419 attachment that has no effect on nuclease activity (**Supplementary figure 3**). Since ColE9  
 420 import is dependent on the PMF and delivery of the PMF occurs via the N-terminal regions  
 421 of the colicin, these results can only be explained if the entire colicin passes through the  
 422 eyelet of the porin carrying the fluorophore with it.

423 The differential effects of fluorophores on ColE9 toxicity and import in cells harbouring  
 424 OmpC or OmpF raised the question of why, when the dimensions of porin eyelets are similar,  
 425 bulky fluorophores pass apparently unhindered through OmpF? We hypothesized that the  
 426 long time-course (overnight) of the cell-killing assays might mask the import effects of bulky  
 427 fluorophores on *E. coli* cells expressing *ompF*. To determine if more subtle effects were  
 428 evident on shorter timescales the kinetics of killing *E. coli* JW2203 cells, which only express  
 429 *ompF*, were determined after addition of ColE9 K469C labelled with AF488, AF568 or AF647  
 430 (**Figure 6e**). The kinetics of cell death were monitored by measuring colony forming units

(CFUs) as a function of time, following the addition of trypsin to degrade extracellular colicin. Chloramphenicol was used throughout these experiments as a bacteriostatic agent to stop cell division, which would otherwise complicate interpretation of cell-death kinetics. The data in **Figure 6e** demonstrate that the ColE9-mediated killing of *ompF*-expressing cells showed a first-order kinetic profile regardless of which fluorophore is attached. The fluorophores nevertheless had a profound impact on the half-life of this process; the half-life for cell-death by unlabelled ColE9 was ~2.5 min, at 37°C, which increased almost two-fold for ColE9 K469C<sup>AF488</sup>, ~10-fold for ColE9 K469C<sup>AF647</sup> and ~30-fold for ColE9 K469C<sup>AF568</sup>. The relative order of fluorophore impact on the killing half-life (AF568>AF647>AF488) was the same as the order observed in the plate killing assay with *E. coli* JM83 cells (**Supplementary figure 4**) and the induction of the SOS response in *E. coli* DPD1718 cells (**Supplementary figure 5**), where both strains express *ompF* and *ompC*. In conclusion, the kinetic profiles shown in **Figure 6e** reflect the rate-limited, energised transport of ColE9 molecules through the lumen of a single OmpF subunit following assembly of the OM translocon, which is a concept that is further explored in the Discussion.

## 457 **Discussion**

458

### 459 **Model for the force-dependent import of ColE9 through OmpF**

460 Combining cryo-EM structure determination of ColE9 translocon complexes with  
461 fluorescence microscopy data, and in conjunction with past biochemical, biophysical and  
462 structural data on this and related colicins, it is finally possible to unravel the complex  
463 interplay of passive and active processes at play in the entry mechanism of Tol-dependent  
464 colicins (**Figure 7**).

465 Past work has shown that E group colicins assemble their OM translocons by first  
466 binding with nM affinity to BtuB at a 45° angle relative to the plane of the membrane from  
467 where the N-terminal IUTD captures a neighbouring OmpF (**Figure 7a**) (Housden et al.,  
468 2005; Kurisu et al., 2003). The cryo-EM structure of the intact ColE9 translocon reveals that  
469 the colicin also has to overcome a 35° tilt of BtuB relative to OmpF, which it does by having  
470 an R-domain with long enough reach. From this overhanging position, the IUTD associates  
471 with the pore of an OmpF subunit (designated subunit 2 in our structure), most likely due to  
472 its high local concentration and electrostatic attraction between the pore which is mildly  
473 cationic selective and the N-terminus of the colicin. The disordered polypeptide chain then  
474 reptates through subunit 2 of OmpF to deliver the TBE to the periplasm, capturing TolB at  
475 the expense of its endogenous binding partner, the OM lipoprotein Pal (**Figure 7b**) (Bonsor  
476 et al., 2007; Bonsor et al., 2009). ColE9 mimics the interactions of Pal, unlike Pal however  
477 the colicin induces TolB to expose its N-terminus which houses the TolA binding site.  
478 Concomitant with (or following) binding to TolB, the ColE9 OBS1 sequence inserts into  
479 subunit 1 of OmpF and OBS2 becomes stably bound within subunit 2. The R-domain of  
480 ColE9 dissociates from BtuB thereby accommodating OmpF threading and removing an  
481 architectural constraint on the repositioning of its T-domain, from a central position above  
482 OmpF to one that is now directly above subunit 2 (**Figure 7c**). OmpF threading is also

483 accompanied by rotation of the ColE9 TBE-TolB complex in the periplasm and formation of  
 484 additional stabilising interactions between the colicin and the porin, all of which position the  
 485 ColE9 TBE-TolB complex close to the periplasmic entrance of OmpF subunit 2. It is at this  
 486 point that optimal engagement between PMF-linked TolQ-TolR-TolA in the inner membrane  
 487 and the ColE9 TBE-TolB complex likely occurs (**Figure 7c**). The physiological role of the  
 488 TolQ-TolR-TolA assembly is to drive dissociation of TolB-Pal complexes at the OM,  
 489 releasing Pal to bind the cell wall (Szczepaniak et al., 2020). As a consequence of this PMF-  
 490 driven cycle, TolB is thought to be pulled through the cell wall by TolA. Hence, by virtue of  
 491 its association with TolB, ColE9 is dragged unfolded into the periplasm through subunit 2 of  
 492 OmpF, its C-terminal DNase domain the last to enter the cell (**Figure 7d, e**). Previous colicin  
 493 translocation models have suggested Tol-dependent bacteriocins remain associated with  
 494 their OM components while killing the cell (Benedetti et al., 1992; Duche, 2007). Our data  
 495 suggest this is unlikely to be the case. The entire ColE9 molecule enters the periplasm,  
 496 driven by interactions at its N-terminus with the PMF-driven Tol-Pal system. Subsequent  
 497 transport of the nuclease domain across the inner membrane requires the  
 498 AAA<sup>+</sup>ATPase/protease FtsH. FtsH also proteolytically processes the domain as it enters  
 499 the cytoplasm, although the underlying mechanism is unknown (Chauleau et al., 2011;  
 500 Walker et al., 2007).

501 Forced unfolding of ColE9 during OM transport is consistent with several lines of  
 502 evidence. First, our cryo-EM data. The structural changes that accompany ColE9  
 503 translocon formation, in which the T-domain and ColE9 TBE-TolB complex become aligned  
 504 over the same OmpF subunit, suggest they are the means by which the bacteriocin  
 505 maximises its access to PMF-mediated force transduction through OmpF. Second, internal  
 506 disulphide bonds within the coiled-coil domain block ColE9 entry, which can be explained  
 507 by the crosslinks blocking the unfolding necessary to allow entry through OmpF (Penfold et  
 508 al., 2004). Third, *in vivo* experiments have shown that release of Im9 (which forms a fM

509 complex with the E9 DNase) at the cell surface is dependent on the electrical potential of  
 510 the PMF (Vankemmelbeke et al., 2013), which is also the case for the entry of fluorescently-  
 511 labelled ColE9 in our experiments. These observations are consistent with the release of  
 512 Im9 accompanying the force-dependent unfolding and import of the colicin DNase through  
 513 OmpF. Fourth, *in vitro* atomic force microscopy measurements have demonstrated that  
 514 when forces equivalent to those attainable by the PMF are applied to the isolated ColE9  
 515 DNase-Im9 complex the DNase domain melts, releasing Im9 but only when the force is  
 516 applied at the N-terminus of the domain (Farrance et al., 2013). Viewed in the context of a  
 517 translocating ColE9 molecule at the OM, the force exerted by the PMF would similarly be  
 518 applied at the N-terminus of the toxin, with the surface of OmpF acting as the barrier against  
 519 which the toxin is unfolded and Im9 displaced.

520 We conclude that the transport mechanism uncovered for ColE9 is likely to be the  
 521 basis for the import of most Tol-dependent bacteriocins, the majority of which require porins.  
 522 This will certainly be the case for E group nuclease colicins (E2-E9) that use BtuB as their  
 523 receptor, and share high sequence identity with ColE9, but deliver rRNases or tRNases as  
 524 well as DNases into the cell. This is also likely to be the case for pore-forming bacteriocins  
 525 such as ColA, ColK and ColN, which use porins as translocators but different OM receptors  
 526 (Kleanthous, 2010).

527

## 528 **Ton- and Tol-dependent bacteriocins exploit analogous PMF-dependent mechanisms** 529 **to cross the outer membrane through protein pores**

530 The basic import principles we have uncovered for ColE9 highlights similarities with  
 531 those recently described for the Ton-dependent bacteriocins pyocins S2 and S5, which  
 532 target *Pseudomonas aeruginosa*. Both S2 and S5 associate with the common  
 533 polysaccharide antigen on the cell surface and then exploit different TBDTs, FpvAI and FptA,  
 534 respectively, as translocators to the periplasm (Behrens et al., 2020; White et al., 2017).

Translocation of these bacteriocins involves two energised events. The first displaces the plug domain that occludes the central pore of the TBDT by a TonB-dependent mechanism, akin to that accompanying ligand uptake through the transporter. The second involves transport of the unfolded toxin through the now-open TBDT pore following delivery of the toxin's N-terminal TonB box to the periplasm. The mechanism we describe for Tol-dependent bacteriocins is analogous to the second of these steps. The similarity is underscored by the way in which force is exerted by TonB and TolA on their endogenous OM protein targets. The C-terminal domains of both proteins form structurally related, parallel  $\beta$ -sheets with their partners involving  $\beta$ -strand augmentation; TonB with the N-termini of TBDTs, TolA with the N-terminus of TolB (Pawelek et al., 2006; Szczepaniak et al., 2020). Such complexes are resistant to mechanical deformation (Chen et al., 2015). Hence, when the PMF-coupled stators ExbB-ExbD and TolQ-TolR, respectively, exert force on them instead of dissociating they remain bound, descending towards the inner membrane as TonB and TolA retract (Hickman et al., 2017). By hijacking these systems, both Ton- and Tol-dependent bacteriocins use the PMF to import themselves across the OM in unfolded form through either pre-existing pores (porins) or pores opened transiently by the PMF (TBDTs).

## **Rate-limited transport of ColE9 through porins can be used to import large chemical entities into *E. coli***

The single-hit kinetic profiles observed for colicin-mediated killing of *E. coli* have been known since the 1960s (Reeves, 1965). However, the basis of this characteristic phenomenon has remained elusive. Our data reveal that this kinetic behaviour reflects the rate-limited transport of the colicin through the OM. The cell-killing half-life for ColE9 targeting *E. coli* cells with OmpF as the only porin in the OM (~2.5 min at 37 °C and pH 7.5) changes significantly when AlexaFluor dyes are attached to the DNase domain, by up to 30-

fold in the case of AF568. We suggest that much of this additional time reflects repeated attempts by the Tol-Pal system, in conjunction with the PMF, to bring this single, bulky, negatively-charged adduct through the narrow eyelet of OmpF subunit 2 (**Figure 6e**). The task of bringing this adduct through OmpC becomes even greater because of the eyelet's greater negative charge.

Glycopeptide antibiotics like vancomycin do not kill Gram-negative bacteria because they cannot partition into the OM and are too large to diffuse through porins. This impermeability problem is a major factor in multidrug resistance amongst Gram-negative pathogens. One approach being developed to circumvent these issues is to conjugate such complex antibiotics to siderophores (so-called Trojan horse antibiotics) so that they can be actively transported through specific TBDTs, energised by the PMF-linked Ton-system (Klebba et al., 2021). Our data show that large, bulky, organic fluorophores that approach the size and complexity of vancomycin can be actively transported through the porins of *E. coli* by piggy-backing on a colicin. Colicins might therefore represent a new vehicle for the delivery of antibiotics that cannot otherwise penetrate the OM of Gram-negative bacteria.

## 586 **Acknowledgements**

587 We are indebted to Patrice Rassam (Strasbourg) and Patricks Inns (Oxford) for help and  
 588 advice regarding microscopy experiments, David Staunton (Molecular Biophysics Suite,  
 589 Oxford) for help with biophysical analysis of purified and fluorescently-labelled proteins, and  
 590 Jeremy Keown and Loic Carrique for assistance with computational analysis of cryo-EM  
 591 data. Cryo-EM data for this investigation were collected at the ISMB EM facility at Birkbeck  
 592 College, University of London with financial support from Wellcome Trust (202679/Z/16/Z  
 593 and 206166/Z/17/Z). The work was funded by the European Research Council (Advanced  
 594 grant 742555; OMPorg) and the Wellcome Trust (201505/Z/16/Z). MLRF was supported by  
 595 the BBSRC Oxford Interdisciplinary Bioscience DTP. We are also indebted to Nadia Halidi  
 596 and the Micron Advanced Bioimaging Unit (Wellcome Strategic Awards 091911/B/10/Z and  
 597 107457/Z/15/Z) for their support & assistance in this work. We thank the Oxford Biomedical  
 598 Research Computing (BMRC) facility, a joint development between the Wellcome Centre  
 599 for Human Genetics and the Big Data Institute (supported by Health Data Research UK and  
 600 the NIHR Oxford Biomedical Research Centre).

601

## 602 **Author contributions**

603 N.G.H, M.N.W., M.L.R.F, N.L. and C.K. designed research; R.K., E.E. and B.C. provided  
 604 materials; M.L.R.F., M.N.W., and N.L. performed research; M.L.R.F and M.N.W. analysed  
 605 data; C.K. and M.N.W. wrote the paper.

606

## 607 **Conflicts of Interest Statement**

608 The authors confirm they have no conflicts of interests

609

## 610 **Data Availability Statement**

611 The data supporting the findings of the study are available in the article, available upon  
612 request from the corresponding author or submitted to the protein structure data bank (PDB).  
613

## 614 **Materials and Methods**

615

### 616 *Plasmids, bacterial strains and media*

617 Whole plasmid site-directed mutagenesis was used to introduce a solvent accessible  
618 cysteine K469C in the cytotoxic domain of ColE9.Im9His6, cloned into pET21a to give  
619 pMLF07. pMLF07 was used to introduce H551A within the cytotoxic domain to give pMLF08,  
620 a cytotoxic inactive construct. Plasmid pEE01 was used to express ColB-His6 in  
621 pACYCduet-1. Plasmid pBC1 expressing ColE9 DNase K469C.Im9His6, containing ColE9  
622 DNase domain with K469C single cysteine, in pET21d, was generated from pRJ353.  
623 Plasmid pREN151 was amplified from a pCS4 derivative and inserted between NdeI and  
624 XhoI sites of pET21a to enable expression and purification with C-terminal His6 tag. All *E.*  
625 *coli* strains and plasmids used in this study are listed in supplementary tables 2 and 3.  
626 Strains were routinely grown at 37 °C in either Lysogeny broth (LB) (Miller 1972) or M9-  
627 minimal media or plated on LB-agar. Supplemented M9-minimal media contained 47.78 mM  
628 Na<sub>2</sub>HPO<sub>4</sub>, 22 mM KH<sub>2</sub>PO<sub>4</sub>, 8.56 mM NaCl, 2 mM MgSO<sub>4</sub>, 0.1 mM CaCl<sub>2</sub>, 18.7 mM NH<sub>4</sub>Cl,  
629 0.4 % (w/v) D-glucose, 0.05% (w/v) casamino acids and 0.0002 % (w/v) thiamine.

630

### 631 *Protein purification*

632 ColE9 and TolB variants were expressed and purified as described previously  
633 (Garinot-Schneider et al., 1997; Garinot-Schneider et al., 1996b; Housden et al., 2013;  
634 Loftus et al., 2006). Plasmids encoding protein of interest were expressed in *E. coli* BL21  
635 (DE3) cells grown in shaking LB flasks at 37 °C (supplemented with 100µg/ml ampicillin) to  
636 an OD<sub>600</sub> of 0.7 and protein expression induced with 1 mM isopropyl-β-D-1-  
637 thiogalactopyranoside (IPTG). Cells were grown for a further 3 h, then harvested by  
638 centrifugation, re-suspended in binding buffer (20 mM potassium phosphate pH 7, 500 mM  
639 NaCl, 5 mM imidazole) supplemented with 1 mM PMSF (and 10mg lysozyme for pMLF07/08)  
640 and lysed by sonication. The soluble cell lysate obtained after centrifugation was loaded

641 onto a 5 ml HisTrap FF HP nickel column (GE Healthcare) equilibrated with binding buffer.  
 642 CoIE9 K469C and CoIE9 H551A K469C were eluted from column-bound His-Im9 through  
 643 denaturation with guanidine hydrochloride (20 mM potassium phosphate pH 7, 500 mM  
 644 NaCl, 6 M guanidine pH 7). Eluted fractions were analysed by SDS-PAGE to locate protein  
 645 before overnight dialysis into SEC buffer to refold protein (20 mM potassium phosphate pH  
 646 7, 500 mM NaCl) supplemented with 10 mM DTT. For CoIE9 W39A and CoIE9 R-domain  
 647 (pNGH96 and pRK151) were eluted using a linear imidazole gradient from 50-250 mM over  
 648 10 column volumes. Following SDS-PAGE analysis, the pooled sample was spiked with  
 649 EDTA (5 mM) and dialysed overnight into SEC buffer containing 20 mM Tris/HCl pH 7.5,  
 650 150 mM NaCl. Proteins were further purified by SEC, using a Superdex 200 Hiload 26/600  
 651 column (GE Healthcare) equilibrated with SEC buffer (10 mM DTT added to buffer where  
 652 CoIE9 contained free cysteine residue). Protein concentrations were determined by UV  
 653 absorbance at 280 nm using sequence-based extinction coefficient (Gill and von Hippel,  
 654 1989).

655

#### 656 *Preparation of the CoIE9 translocon for Cryo-EM*

657 Intact CoIE9 translocon complex was prepared as previously described (Housden et  
 658 al., 2013). The purified CoIE9 translocon in 20 mM MES pH 6.5 and 1%  $\beta$ -OG (100  $\mu$ L),  
 659 was diluted 10-fold into buffer containing 20 mM potassium phosphate, pH 7.9, 100 mM  
 660 NaCl and 1%  $\beta$ -OG. Amphipol was added to protein in a ratio of 10 mg amphipol:1mg  
 661 protein, and the sample was left to incubate at room temperature for 2 hr. Detergent was  
 662 removed through the addition of BioBeads (Bio-Rad) at a ratio of 10 mg beads to 1 mg of  
 663 detergent. After a 2 hr incubation at room temperature, the sample was injected onto a  
 664 superose 6 increase 10/300 column, equilibrated in 20 mM potassium phosphate, pH 7.9,  
 665 100 mM NaCl. Fractions were analysed by SDS-PAGE to validate all components of the  
 666 complex were present, before spin concentrating the sample to 2.0 mg/ml.

667 The quality and concentration of samples were confirmed by negative stain EM prior to cryo-  
668 EM sample preparation. C-flat grids (Protochips, USA; 1.2/1.3 300 mesh) and UltrAuFoil  
669 (Quantifoil, Germany; 1.2/1.3 300 mesh) were negatively glow discharged using PELCO  
670 Easiglow (Ted Pella, USA) and coated with graphene oxide as described previously (Wang  
671 et al., 2020). Prior to application to graphene coated quantifoil grids, translocon preparation  
672 was diluted to 0.05 mg/ml with buffer containing 20 mM potassium phosphate, pH 7.9, 100  
673 mM NaCl. 3  $\mu$ L of sample was applied to grid and vitrified in liquid ethane using a Vitrobot  
674 Mark IV (Thermo Fisher Scientific, USA) at 4°C and 94% humidity.

675

# 676 *Cryo-EM image collection and processing*

677 Cryo-EM data were collected in ISMB Birkbeck EM facility using a Titan Krios  
678 microscope (Thermo Fisher Scientific, USA) operated at 300 keV and equipped with a  
679 BioQuantum energy filter (Gatan, USA). The images were collected with a post-GIF K2  
680 Summit direct electron detector (Gatan, USA) operated in counting mode, at a nominal  
681 magnification of 130,000 corresponding to a pixel size of 1.047 Å. The dose rate was set to  
682 4.99 e Å<sup>2</sup> per second, and a total dose of 49-50 e/Å<sup>2</sup> was fractionated over 50 frames. An  
683 energy slit with a 20 eV width was used during data collection. Data were collected using  
684 EPU software with a nominal defocus range -1.5  $\mu$ m to -3.5  $\mu$ m. Relion 3.1 software  
685 package (Scheres, 2012a, b; Zivanov et al., 2018; Zivanov et al., 2020) was used for data  
686 motion correction and dose weighting with MotionCor2 (Zheng et al., 2017). Data were then  
687 imported into cryoSPARC (Punjani et al., 2017; Punjani et al., 2020) and the contrast  
688 transfer function (CTF) estimated using GCTF (Zhang, 2016). After removing micrographs  
689 with non-vitreous ice, broken graphene oxide support or poor CTF fit, blob picking followed  
690 by particle extraction, and 2D classification were used to generate templates for template-  
691 based picking within cryoSPARC. Template-picked particles were extracted with a 280-

692 pixel box and sorted using 2D classification. From here, the processing workflow for the two  
693 datasets diverged.

694 For data set one (654,865 particles), five *ab initio* classes were generated following  
695 2D classification, and classes were refined using heterologous refinement within  
696 cryoSPARC. In two of the resulting classes, the density was consistent with a translocon  
697 complex, these were selected for further processing using non-uniform refinement, prior to  
698 import into relion3.1. After 3D refinement the full translocon map reported an overall  
699 resolution of 5.0 Å and the partial translocon map, 3.7 Å. To improve the quality of the partial  
700 translocon map the detergent shell was subtracted and the resulting particles were refined  
701 to generate a new map with a reported resolution of 3.9 Å. In parallel to 3D refinement  
702 subtracted particles were also further sorted using a 3D classification step, without alignment  
703 and sorting into four classes. All four classes were refined independently, with only one  
704 class showing map density for both ColE9 and TolB. After a 3D refinement of this class, a  
705 map was generated with a reported resolution of 3.7 Å which, following post-processing and  
706 local resolution estimation, was sharpened using either LocScale (Jakobi et al., 2017) or  
707 deepEMhancer (Sanchez-Garcia et al., 2020). Visual inspection of the sharpened maps  
708 confirmed the selection of the deepEMhancer tight map (**Supplementary figure 1**) as the  
709 final map for the partial translocon. Similar sorting and refinement procedures were applied  
710 to the full translocon particles, however no improvements in map resolution and quality were  
711 observed.

712 Data set two (434,671 particles after 2D classification) was processed using  
713 cryoSPARC. Three *ab initio* maps were generated and subject to heterologous refinement.  
714 Of these classes only one class showed weak density for both TolB and ColE9, at higher  
715 threshold levels, in addition to the density consistent with the OmpF trimer. This map was  
716 then further processed using non-uniform refinement. The resulting map reported a  
717 resolution of 3.2 Å, however upon visual inspection of the map it revealed poor density for

718 TolB and ColE9 relative to the partial translocon map from dataset one, and also had non-  
719 isotropic density within OmpF, therefore no further processing was carried out.

720 After independent processing of both datasets, the particles were combined to give  
721 1,089,536 particles which were sorted using a second 2D classification step. Classes were  
722 divided into three groups, full translocon, partial translocon, and junk. The particles in the  
723 full and partial translocon classes were independently processed within cryoSPARC. Two  
724 maps of the full translocon were generated from *ab initio* reconstruction. One map had a  
725 more intact structure with density for all components and was therefore refined further using  
726 non-uniform refinement, to give a map with a reported resolution of 4.0 Å. Visual inspection  
727 of the map showed that only the OmpF portion of the map extended to 4.0 Å with the majority  
728 of the remaining map having poorly resolved secondary structure and weak density  
729 associated with ColE9 and TolB. To improve the quality of the map, the detergent shell was  
730 subtracted and the map locally refined. This generated a map with a reported resolution of  
731 4.6-16 Å, however the density of ColE9 and TolB had improved. This map was sharpened  
732 with either LocScale or deepEMhancer, with the deepEMhancer tight mask map generating  
733 the final map of the full translocon. To assess the degree of conformational heterogeneity,  
734 3D variability analysis was implemented using particles input into the final map. From the  
735 analysis five maps were generated, which showed movement within TolB and ColE9.  
736 Comparison of these maps with that of the partial translocon, did not show a map whereby  
737 the conformation of ColE9 or TolB matched that seen in the partial translocon map,  
738 suggesting that the partial translocon and full translocon were discrete states.

739 After combining datasets, particles assigned to the partial translocon class were  
740 processed using a similar method to that applied to the full translocon above. Four classes  
741 were generated from *ab initio* reconstruction and heterologous refinement. Of these four  
742 classes only one showed density for both ColE9 and TolB, this class was processed further  
743 using non-uniform refinement, local refinement, detergent shell subtraction, and a final local

744 refinement step, to generate a map with a reported resolution of 3.6 Å. This map was input  
745 into 3D variability analysis generating five maps to assess the degree of conformational  
746 heterogeneity. Once again density for ColE9 consistent with the full translocon map was  
747 absent.

748 To build a partial translocon model OmpF (PDB ID 3K19), was docked into the partial  
749 translocon map from relion using chimera (Pettersen et al., 2004) and rigid-body refined  
750 using Phenix (Afonine et al., 2018a; Afonine et al., 2018b; Liebschner et al., 2019). ColE9  
751 residues 2-75 were manually built into the remaining map density present within the OmpF  
752 pores within coot (Emsley and Cowtan, 2004) and several cycles of rigid-body and local  
753 refinement was carried out using Phenix. TolB-ColE9 32-47 (PDB ID 2IVZ) was then docked  
754 into map using chimera and rigid body refined using phenix. Due to the weak density in the  
755 TolB portion of the map, the ColE9 peptide was not clearly resolved, however after rigid-  
756 body fitting the terminal residues (32 and 47) were proximal to the ColE9 chain built prior to  
757 TolB docking. Therefore, residues 32-47 of ColE9 bound in the TolB crystal structure were  
758 substituted for *ab initio* built sequence and the whole complex (OmpF, TolB and ColE9  
759 residues 2-75) refined using phenix. Only rigid body refinement was applied to the TolB  
760 portion of the map due to the lower resolution in this region of the map. The ColE9 T-domain  
761 residues 85-314 (PDB ID 5EW5) was docked into the map using chimera, merged with  
762 remaining parts of the translocon, and rigid body refined in phenix to give the final partial  
763 translocon model. Due to the weak density following on from ColE9 residue 75 the  
764 disordered N-terminal domain could not be reliably built past this point to connect residues  
765 75 and 85.

766 For the full translocon model, OmpF and ColE9 residues 2-75 from the partial  
767 translocon structure were docked into the final full translocon map within chimera.  
768 Additionally, BtuB bound to the R-domain of ColE3 (PDB ID 2YSU) was also docked into  
769 the map, prior to running refinement within Phenix. Only rigid body refinements were run

for this model due to the lower resolution of the map. The crystal structure of ColE9 (PDB ID 5EW5) was docked into the map, through alignment to the R-domain of ColE3 within chimera. This created an anchor point for the R-domain that prevented steric clashes with BtuB. The TolB-ColE9 32-47 crystal structure was once again docked into the map and merged with ColE9 2-75, and the whole complex rigid-body refined in phenix, to generate the final model.

Map to model parameters from Phenix, model validation and map processing workflow are summarised in **Supplementary Figures 1-3** and **Supplementary Table 1**. Structure representation figures were made using chimeraX (Goddard et al., 2018; Pettersen et al., 2021) and pymol.

#### *Vitamin B<sub>12</sub> competition assay*

The assay was carried out as described previously (Penfold et al., 2000). In brief, *E. coli* 133/3 cells grown overnight in 5 ml minimal media (1x M9 salts, 100 µg/ml L-arginine, 1 mM MgSO<sub>4</sub>, 0.2% glucose) and supplemented with vitamin B<sub>12</sub> (1 nM), prior to dilution 1:100 in 50 ml of minimal media containing vitamin B<sub>12</sub> (1 nM) and ColE9 R-domain or ColE9 W39A (40 nM). Cells were maintained at 37 °C with shaking for a total time of 6 hours. Samples (1 ml) were removed every 30 minutes and optical density at 600 nm (OD<sub>600</sub>) recorded. Average OD<sub>600</sub> values and standard deviation across triplicate measurements are reported.

#### *Colicin cytotoxicity assay*

Colicin cytotoxicity was assayed by plate-based growth inhibition assays that were carried out as described previously (Atanaskovic et al., 2020; Jansen et al., 2020). An overnight culture of *E. coli* was used to inoculate LB (5-10 ml, containing appropriate antibiotics) and grown at 37 °C until reaching an OD<sub>600</sub> ~0.4. 200 µL of culture was added

796 to 5 ml of molten soft LB-agar (0.75 % (w/v)) at 45 °C, mixed by inversion and poured over  
797 LB-agar plates (supplemented with appropriate antibiotics) and allowed to cool and dry.  
798 Serial dilutions of colicin were spotted onto the plate (2 µl) and incubated at 37 °C overnight.  
799 Colicin induced cell killing was indicated as zones of clearance in the bacterial lawn.

#### 800 *Fluorophore labelling of proteins*

801 Single cysteine mutants of ColE9 or the ColE9 DNase domain were desalted on a 5  
802 ml HiTrap column (GE Healthcare) equilibrated with binding buffer (20 mM potassium  
803 phosphate pH 7, 500 mM NaCl) to remove DTT. The protein was diluted to 50 µM and  
804 labelled with a 5:1 molar excess of fluorophore:protein with either AlexaFluor 488 C<sub>5</sub>-  
805 Maleimide (Invitrogen) (AF<sup>488</sup>), AlexaFluor 568 C<sub>5</sub>-Maleimide (Invitrogen) (AF<sup>568</sup>), or  
806 AlexaFluor 647 C<sub>2</sub>-Maleimide (Invitrogen) (AF<sup>647</sup>). Maleimide dyes were re-suspended in  
807 DMSO and stored as a 10 mM stock. Labelling was allowed to proceed for 1-2 hours at  
808 room temperature in the dark, and then quenched using 2 mM DTT for 15 min, before  
809 overnight dialysis at 4°C (20 mM potassium phosphate pH 7, 500 mM NaCl) to remove  
810 excess dye (Spectra Por 10K MWCO). Labelled protein was applied to a Superdex 200  
811 10/300 GL column (GE Healthcare) equilibrated with 20 mM potassium phosphate pH 7,  
812 500 mM NaCl, to remove residual dye. Protein-containing fractions were identified by SDS-  
813 PAGE. The protein concentration and labelling efficiency (typically >90%) was estimated  
814 from absorbance readings using sequence-based extinction coefficients, molecular weights,  
815 and dye correction factors (Invitrogen)

816

#### 817 *Plasmid nicking assay*

818 pUC19 DNA was used at 1 µg/ml in 50 mM triethanolamine (Fisher Scientific) pH 7.5  
819 with 20 mM MgCl<sub>2</sub> and 200 nM ColE9 DNase domain. 5 µl samples were taken at timepoints,  
820 the reaction quenched with EDTA (37.5 mM, pH 8.0) and products separated on an agarose  
821 gel (1.2 %) following the addition DNA loading dye (Invitrogen).

822

823 *Bioluminescence assay*

824 *E. coli* DPD1718 cells were inoculated from an overnight culture, into 10 ml LB and  
 825 grown at 37 °C until OD<sub>600</sub> ~0.4. Cells were diluted 1:2 in 100 µl with warmed LB (37 °C),  
 826 into a black Nunc microwell 96 well optical bottom polystyrene plate. ColE9 was used at 0,  
 827 0.5, 1, 2, and 20 nM. The plate was loaded into a plate incubator (Freedom Evo 150 robot)  
 828 at 37 °C with gentle shaking. After loading of plates into Tecan Infinite M200 Pro plate  
 829 reader cell growth (600 nm) and bioluminescence (490 nm) measured every 10 minutes.

830

831 *Cell preparation for live cell imaging by fluorescence microscopy*

832 *E. coli* cells from an overnight LB culture were used to inoculate 10 ml of  
 833 supplemented M9 minimal media (with the appropriate antibiotics) and grown at 37 °C until  
 834 they reached OD<sub>600</sub> of 0.4. Cells (1.6 ml) were pelleted by centrifugation (7000 g for 3 mins  
 835 at 17 °C), and re-suspended in 200 µl M9 containing 1.5 µM of fluorescently-labelled colicin  
 836 and 20 µM Hoechst 33342 (Thermofisher). Cells were incubated for 30 minutes at room  
 837 temperature with rotary inversion in the dark, then pelleted by centrifugation and re-  
 838 suspended in 400 µl supplemented M9 minimal media. Pelleting followed by resuspension  
 839 was repeated twice more to remove unbound label. Finally, pelleted cells were re-  
 840 suspended in a small volume (10-100 µl) of M9 and 10 µl loaded onto 1% (w/v) M9 minimal  
 841 media agarose pad using a 1.5 x 1.6 cm Gene Frame matrix, solidified on a 1.2-1.5 mm  
 842 thick microscope slide (Thermo Fisher).

843 For CCCP experiments, pelleted cells were re-suspended in 400 µl of 100 µM CCCP  
 844 (Sigma) and incubated for 5 minutes at room temperature prior to the addition of ColE9.  
 845 CCCP remained present in media throughout wash steps and in the agarose pad. For  
 846 nigericin and valinomycin experiments, cells were permeabilised using 1 mM EDTA pH 8.0  
 847 for 5 minutes before treatment with 5 µM nigericin (Sigma) or 5 µM valinomycin (Sigma) in

the presence of 150 mM KCl, and incubated for 5 minutes at room temperature, to inhibit the proton concentration gradient ( $\Delta\text{pH}$ ) or the electrical potential ( $\Delta\Psi$ ), respectively, before addition of colicin. Nigericin and valinomycin remained present throughout the washes and in the agarose pad.

For trypsin experiments, labelled and washed cells were re-suspended in 200  $\mu\text{l}$  M9 media containing trypsin (Sigma) to achieve a 2:1 colicin:trypsin ratio. Cells were incubated with trypsin for 1 h at room temperature with rotary inversion before washing three times in M9.

### *Widefield microscopy data acquisition and analysis*

Live cells were imaged at room temperature using a 60x oil-immersion objective (Oil UPlanSApo) (NA 1.42) on an OMX V3 BLAZE Optical microscope with Deltavision OMX software. The 405 nm (DAPI filter), 488 nm (FITC filter), 593 nm (615/24 filter) or 642 nm (Cy5 filter) laser lines were used. Lasers were used at 10-31.5 % laser intensities and an exposure time of 30 ms. Differential interference contrast (DIC) was used to image the cell. The fluorescence channels were used to acquire single images, recorded at a frame rate of 30 ms/frame.

Widefield data in the fluorescence channels (405 nm, 488 nm, 593 nm and 642 nm) were smoothed using ImageJ (Schneider et al., 2012). The data were normalised and set at a minimum of  $\sim 100$  units/pixels to remove background. Fluorescence intensity distribution across the width of cells was determined using ImageJ (Schneider et al., 2012) plot profile function. A total of 15 cells for each condition were analysed and the average plotted with the standard error of mean (SEM). Image intensity quantification was obtained by drawing cell outlines and determining the mean pixel intensity from the 16-bit images within ImageJ. A total of 37-126 cells were analysed per condition.

874 *E. coli cell death kinetics*

875 *E. coli* JW2203 (OmpF-expressing) cells (25 ml) were grown in LB at 37 °C to OD<sub>600</sub>  
 876 ~0.4 (~10<sup>8</sup> cells) prior to addition of chloramphenicol (20 µg/ml), to inhibit cell division, and  
 877 either wild-type ColE9 or ColE9 K469C labelled with AF488, AF568 or AF647 (80 nM) added  
 878 to the culture. A no-colicin control was also included. Colicin import was stopped at specific  
 879 time points by removing 900 µl of culture and adding 100 µl of trypsin (1 mg/ml) and  
 880 incubated at 37 °C for 30 min. 100 µl of each sample was diluted in LB (10<sup>0</sup> -10<sup>6</sup> fold),  
 881 before plating (90 µl) on LB-agar plates (with appropriate antibiotics), and incubating for 16  
 882 hours at 37 °C. Colonies were counted and averaged from across triplicate plates. The  
 883 number of CFUs were calculated using the following equation:

884  $CFU = \text{average number of colonies} \times \text{dilution factor} / \text{volume plated (ml}^{-1}\text{)}$

885 The natural log of each CFU value was plotted against time (mins), and the rate constant (k)  
 886 of the reaction was calculated by representing the first order reaction as a straight line using  
 887 equation:  $y = kx + c$ . The half-life of the reaction in cell killing kinetics are quoted as  $t_{1/2}$   
 888 values, where  $t_{1/2} = \ln 2/k$ .

889

890

# References

- Afonine, P.V., Klaholz, B.P., Moriarty, N.W., Poon, B.K., Sobolev, O.V., Terwilliger, T.C., Adams, P.D., and Urzhumtsev, A. (2018a). New tools for the analysis and validation of cryo-EM maps and atomic models. *Acta Crystallogr D Struct Biol* 74, 814-840.
- Afonine, P.V., Poon, B.K., Read, R.J., Sobolev, O.V., Terwilliger, T.C., Urzhumtsev, A., and Adams, P.D. (2018b). Real-space refinement in PHENIX for cryo-EM and crystallography. *Acta Crystallogr D Struct Biol* 74, 531-544.
- Aoki, S.K., Diner, E.J., de Roodenbeke, C.T., Burgess, B.R., Poole, S.J., Braaten, B.A., Jones, A.M., Webb, J.S., Hayes, C.S., Cotter, P.A., *et al.* (2010). A widespread family of polymorphic contact-dependent toxin delivery systems in bacteria. *Nature* 468, 439-442.
- Atanaskovic, I., Mosbahi, K., Sharp, C., Housden, N.G., Kaminska, R., Walker, D., and Kleanthous, C. (2020). Targeted Killing of *Pseudomonas aeruginosa* by Pyocin G Occurs via the Hemin Transporter Hcr. *Journal of molecular biology* 432, 3869-3880.
- Baba, T., Ara, T., Hasegawa, M., Takai, Y., Okumura, Y., Baba, M., Datsenko, K.A., Tomita, M., Wanner, B.L., and Mori, H. (2006). Construction of *Escherichia coli* K-12 in-frame, single-gene knockout mutants: the Keio collection. *Mol Syst Biol* 2, 2006 0008.
- Basle, A., Rummel, G., Storici, P., Rosenbusch, J.P., and Schirmer, T. (2006). Crystal structure of osmoporin OmpC from *E. coli* at 2.0 Å. *Journal of molecular biology* 362, 933-942.
- Basler, M., Ho, B.T., and Mekalanos, J.J. (2013). Tit-for-tat: type VI secretion system counterattack during bacterial cell-cell interactions. *Cell* 152, 884-894.
- Behrens, H.M., Lowe, E.D., Gault, J., Housden, N.G., Kaminska, R., Weber, T.M., Thompson, C.M.A., Mislin, G.L.A., Schalk, I.J., Walker, D., *et al.* (2020). Pyocin S5 Import into *Pseudomonas aeruginosa* Reveals a Generic Mode of Bacteriocin Transport. *mBio* 11.
- Benedetti, H., Lloubes, R., Lazdunski, C., and Letellier, L. (1992). Colicin A unfolds during its translocation in *Escherichia coli* cells and spans the whole cell envelope when its pore has formed. *EMBO J.* 11, 441-447.
- Blattner, F.R., Plunkett, G., 3rd, Bloch, C.A., Perna, N.T., Burland, V., Riley, M., Collado-Vides, J., Glasner, J.D., Rode, C.K., Mayhew, G.F., *et al.* (1997). The complete genome sequence of *Escherichia coli* K-12. *Science* 277, 1453-1462.
- Bonsor, D.A., Grishkovskaya, I., Dodson, E.J., and Kleanthous, C. (2007). Molecular Mimicry Enables Competitive Recruitment by a Natively Disordered Protein. *J. Am. Chem. Soc.* 129, 4800-4807.
- Bonsor, D.A., Hecht, O., Vankemmelbeke, M., Sharma, A., Krachler, A.M., Housden, N.G., Lilly, K.J., James, R., Moore, G.R., and Kleanthous, C. (2009). Allosteric beta-propeller signalling in TolB and its manipulation by translocating colicins. *The EMBO journal* 28, 2846-2857.

- 941 Cascales, E., Buchanan, S.K., Duché, D., Kleanthous, C., Lloubès, R., Postle, K., Riley, M.,  
942 Slatin, S., and Cavard, D. (2007). Colicin biology. *Microbiol Mol Biol Rev* 71, 158-229.  
943
- 944 Chauleau, M., Mora, L., Serba, J., and de Zamaroczy, M. (2011). FtsH-dependent  
945 processing of RNase colicins D and E3 means that only the cytotoxic domains are imported  
946 into the cytoplasm. *The Journal of biological chemistry* 286, 29397-29407.  
947
- 948 Chen, Y., Radford, S.E., and Brockwell, D.J. (2015). Force-induced remodelling of proteins  
949 and their complexes. *Current opinion in structural biology* 30, 89-99.  
950
- 951 Cooper, P.C., and James, R. (1984). Two new E colicins, E8 and E9, produced by a strain  
952 of *Escherichia coli*. *J.Gen.Microbiol.* 130, 209.  
953
- 954 Cramer, W.A., Sharma, O., and Zakharov, S.D. (2018). On mechanisms of colicin import:  
955 the outer membrane quandary. *The Biochemical journal* 475, 3903-3915.  
956
- 957 Davidov, Y., Rozen, R., Smulski, D.R., Van Dyk, T.K., Vollmer, A.C., Elsemore, D.A.,  
958 LaRossa, R.A., and Belkin, S. (2000). Improved bacterial SOS promoter&Colon;lux fusions  
959 for genotoxicity detection. *Mutat Res* 466, 97-107.  
960
- 961 Davis, B.D., and Mingioli, E.S. (1950). Mutants of *Escherichia coli* requiring methionine or  
962 vitamin B12. *Journal of bacteriology* 60, 17-28.  
963
- 964 Duche, D. (2007). Colicin E2 is still in contact with its receptor and import machinery when  
965 its nuclease domain enters the cytoplasm. *Journal of bacteriology* 189, 4217-4222.  
966
- 967 Emsley, P., and Cowtan, K. (2004). Coot: model-building tools for molecular graphics. *Acta*  
968 *crystallographica. Section D, Biological crystallography* D60, 2126-2132.  
969
- 970 Farrance, O.E., Hann, E., Kaminska, R., Housden, N.G., Derrington, S.R., Kleanthous, C.,  
971 Radford, S.E., and Brockwell, D.J. (2013). A force-activated trip switch triggers rapid  
972 dissociation of a colicin from its immunity protein. *PLoS Biol* 11, e1001489.  
973
- 974 Garinot-Schneider, C., Penfold, C.N., Moore, G.R., Kleanthous, C., and James, R. (1997).  
975 Identification of residues in the putative TolA box which are essential for the toxicity of the  
976 endonuclease toxin colicin E9. *Microbiology* 143 ( Pt 9), 2931.  
977
- 978 Garinot-Schneider, C., Pommer, A.J., Moore, G.R., Kleanthous, C., and James, R. (1996a).  
979 Identification of putative active-site residues in the DNase domain of colicin E9 by random  
980 mutagenesis. *J Mol Biol* 260, 731-742.  
981
- 982 Garinot-Schneider, C., Pommer, A.J., Moore, G.R., Kleanthous, C., and James, R. (1996b).  
983 Identification of putative active-site residues in the DNase domain of colicin E9 by random  
984 mutagenesis. *J.Mol.Biol.* 260, 731.  
985
- 986 Gehring, K.B., and Nikaido, H. (1989). Existence and purification of porin heterotrimers of  
987 *Escherichia coli* K12 OmpC, OmpF, and PhoE proteins. *The Journal of biological chemistry*  
988 264, 2810-2815.  
989
- 990 Gill, S.C., and von Hippel, P.H. (1989). Calculation of protein extinction coefficients from  
991 amino acid sequence data. *Analytical Biochemistry* 182, 319-326.  
992

993 Goddard, T.D., Huang, C.C., Meng, E.C., Pettersen, E.F., Couch, G.S., Morris, J.H., and  
 994 Ferrin, T.E. (2018). UCSF ChimeraX: Meeting modern challenges in visualization and  
 995 analysis. *Protein Science* 27, 14-25.  
 996  
 997 Granato, E.T., Meiller-Legrand, T.A., and Foster, K.R. (2019). The Evolution and Ecology of  
 998 Bacterial Warfare. *Current biology : CB* 29, R521-R537.  
 999  
 1000 Hands, S.L., Holland, L.E., Vankemmelbeke, M., Fraser, L., Macdonald, C.J., Moore, G.R.,  
 1001 James, R., and Penfold, C.N. (2005). Interactions of TolB with the translocation domain of  
 1002 colicin E9 require an extended TolB box. *Journal of bacteriology* 187, 6733-6741.  
 1003  
 1004 Heller, K., Mann, B.J., and Kadner, R.J. (1985). Cloning and expression of the gene for the  
 1005 vitamin B12 receptor protein in the outer membrane of *Escherichia coli*. *Journal of*  
 1006 *bacteriology* 161, 896-903.  
 1007  
 1008 Hickman, S.J., Cooper, R.E.M., Bellucci, L., Paci, E., and Brockwell, D.J. (2017). Gating of  
 1009 TonB-dependent transporters by substrate-specific forced remodelling. *Nature*  
 1010 *communications* 8, 14804.  
 1011  
 1012 Housden, N.G., Hopper, J.T., Lukyanova, N., Rodriguez-Larrea, D., Wojdyla, J.A., Klein,  
 1013 A., Kaminska, R., Bayley, H., Saibil, H.R., Robinson, C.V., *et al.* (2013). Intrinsically  
 1014 disordered protein threads through the bacterial outer-membrane porin OmpF. *Science* 340,  
 1015 1570-1574.  
 1016  
 1017 Housden, N.G., Loftus, S.R., Moore, G.R., James, R., and Kleanthous, C. (2005). Cell entry  
 1018 mechanism of enzymatic bacterial colicins: Porin recruitment and the thermodynamics of  
 1019 receptor binding. *Proceedings of the National Academy of Sciences of the United States of*  
 1020 *America* 102, 13849-13854.  
 1021  
 1022 Housden, N.G., Rassam, P., Lee, S., Samsudin, F., Kaminska, R., Sharp, C., Goult, J.D.,  
 1023 Francis, M.L., Khalid, S., Bayley, H., *et al.* (2018). Directional Porin Binding of Intrinsically  
 1024 Disordered Protein Sequences Promotes Colicin Epitope Display in the Bacterial Periplasm.  
 1025 *Biochemistry* 57, 4374-4381.  
 1026  
 1027 Housden, N.G., Wojdyla, J.A., Korczynska, J., Grishkovskaya, I., Kirkpatrick, N., Brzozowski,  
 1028 A.M., and Kleanthous, C. (2010). Directed epitope delivery across the *Escherichia coli* outer  
 1029 membrane through the porin OmpF. *Proceedings of the National Academy of Sciences of*  
 1030 *the United States of America* 107, 21412-21417.  
 1031  
 1032 Jakobi, A.J., Wilmanns, M., and Sachse, C. (2017). Model-based local density sharpening  
 1033 of cryo-EM maps. *eLife* 6, e27131.  
 1034  
 1035 Jansen, K.B., Inns, P.G., Housden, N.G., Hopper, J.T.S., Kaminska, R., Lee, S., Robinson,  
 1036 C.V., Bayley, H., and Kleanthous, C. (2020). Bifurcated binding of the OmpF receptor  
 1037 underpins import of the bacteriocin colicin N into *Escherichia coli*. *Journal of Biological*  
 1038 *Chemistry* 295, 9147-9156.  
 1039  
 1040 Jeanteur, D., Schirmer, T., Fourel, D., Simonet, V., Rummel, G., Widmer, C., Rosenbusch,  
 1041 J.P., Pattus, F., and Pages, J.M. (1994). Structural and functional alterations of a colicin-  
 1042 resistant mutant of OmpF porin from *Escherichia coli*. *Proceedings of the National Academy*  
 1043 *of Sciences of the United States of America* 91, 10675-10679.  
 1044

- 1045 Kleanthous, C. (2010). Swimming against the tide: progress and challenges in our  
1046 understanding of colicin translocation. *Nature reviews. Microbiology* 8, 843-848.
- 1047
- 1048 Kleanthous, C., Kuhlmann, U.C., Pommer, A.J., Ferguson, N., Radford, S.E., Moore, G.R.,  
1049 James, R., and Hemmings, A.M. (1999). Structural and mechanistic basis of immunity  
1050 toward endonuclease colicins. *Nature Structural Biology* 6, 243-252.
- 1051
- 1052 Klebba, P.E., Newton, S.M.C., Six, D.A., Kumar, A., Yang, T., Nairn, B.L., Munger, C., and  
1053 Chakravorty, S. (2021). Iron Acquisition Systems of Gram-negative Bacterial Pathogens  
1054 Define TonB-Dependent Pathways to Novel Antibiotics. *Chemical reviews*.
- 1055
- 1056 Klein, A., Wojdyla, J.A., Joshi, A., Josts, I., McCaughey, L.C., Housden, N.G., Kaminska, R.,  
1057 Byron, O., Walker, D., and Kleanthous, C. (2016). Structural and biophysical analysis of  
1058 nuclease protein antibiotics. *The Biochemical journal* 473, 2799-2812.
- 1059
- 1060 Kurisu, G., Zakharov, S.D., Zhalnina, M.V., Bano, S., Eroukova, V.Y., Rokitskaya, T.I.,  
1061 Antonenko, Y.N., Wiener, M.C., and Cramer, W.A. (2003). The structure of BtuB with bound  
1062 colicin E3 R-domain implies a translocon. *Nature Structural Biology* 10, 948-954.
- 1063
- 1064 Lee, S., Housden, N.G., Ionescu, S.A., Zimmer, M.H., Kaminska, R., Kleanthous, C., and  
1065 Bayley, H. (2020). Transmembrane Epitope Delivery by Passive Protein Threading through  
1066 the Pores of the OmpF Porin Trimer. *Journal of the American Chemical Society* 142, 12157-  
1067 12166.
- 1068
- 1069 Liebschner, D., Afonine, P.V., Baker, M.L., Bunkóczi, G., Chen, V.B., Croll, T.I., Hintze, B.,  
1070 Hung, L.W., Jain, S., McCoy, A.J., *et al.* (2019). Macromolecular structure determination  
1071 using X-rays, neutrons and electrons: recent developments in Phenix. *Acta Crystallogr D*  
1072 *Struct Biol* 75, 861-877.
- 1073
- 1074 Loftus, S.R., Walker, D., Mate, M.J., Bonsor, D.A., James, R., Moore, G.R., and Kleanthous,  
1075 C. (2006). Competitive recruitment of the periplasmic translocation portal TolB by a natively  
1076 disordered domain of colicin E9. *Proc. Natl. Acad. Sci. USA* 103, 12353-12358.
- 1077
- 1078 Ng, C.L., Lang, K., Meenan, N.A., Sharma, A., Kelley, A.C., Kleanthous, C., and  
1079 Ramakrishnan, V. (2010). Structural basis for 16S ribosomal RNA cleavage by the cytotoxic  
1080 domain of colicin E3. *Nat Struct Mol Biol* 17, 1241-1246.
- 1081
- 1082 Nikaido, H. (2003). Molecular basis of bacterial outer membrane permeability revisited.  
1083 *Microbiology and Molecular Biology Reviews* 67, 593-656.
- 1084
- 1085 Pawelek, P.D., Croteau, N., Ng-Thow-Hing, C., Khursigara, C.M., Moiseeva, N., Allaire, M.,  
1086 and Coulton, J.W. (2006). Structure of TonB in complex with FhuA, E. coli outer membrane  
1087 receptor. *Science* 312, 1399-1402.
- 1088
- 1089 Penfold, C.N., Garinot-Schneider, C., Hemmings, A.M., Moore, G.R., Kleanthous, C., and  
1090 James, R. (2000). A 76-residue polypeptide of colicin E9 confers receptor specificity and  
1091 inhibits the growth of vitamin B12-dependent *Escherichia coli* 113/3 cells. *Mol. Microbiol.* 38,  
1092 639.
- 1093
- 1094 Penfold, C.N., Healy, B., Housden, N.G., Boetzel, R., Vankemmelbeke, M., Moore, G.R.,  
1095 Kleanthous, C., and James, R. (2004). Flexibility in the receptor-binding domain of the

enzymatic colicin E9 is required for toxicity against *Escherichia coli* cells. *Journal of bacteriology* **186**, 4520-4527.

Pettersen, E.F., Goddard, T.D., Huang, C.C., Couch, G.S., Greenblatt, D.M., Meng, E.C., and Ferrin, T.E. (2004). UCSF Chimera—A visualization system for exploratory research and analysis. *Journal of Computational Chemistry* **25**, 1605-1612.

Pettersen, E.F., Goddard, T.D., Huang, C.C., Meng, E.C., Couch, G.S., Croll, T.I., Morris, J.H., and Ferrin, T.E. (2021). UCSF ChimeraX: Structure visualization for researchers, educators, and developers. *Protein Science* **30**, 70-82.

Pommer, A.J., Cal, S., Keeble, A.H., Walker, D., Evans, S.J., Kuhlmann, U.C., Cooper, A., Connolly, B.A., Hemmings, A.M., Moore, G.R., *et al.* (2001). Mechanism and cleavage specificity of the H-N-H endonuclease colicin E9. *J.Mol.Biol.* **314**, 735.

Pratt, L.A., Hsing, W., Gibson, K.E., and Silhavy, T.J. (1996). From acids to osmZ: multiple factors influence synthesis of the OmpF and OmpC porins in *Escherichia coli*. *Molecular microbiology* **20**, 911-917.

Punjani, A., Rubinstein, J.L., Fleet, D.J., and Brubaker, M.A. (2017). cryoSPARC: algorithms for rapid unsupervised cryo-EM structure determination. *Nature Methods* **14**, 290-296.

Punjani, A., Zhang, H., and Fleet, D.J. (2020). Non-uniform refinement: adaptive regularization improves single-particle cryo-EM reconstruction. *Nature Methods* **17**, 1214-1221.

Ranf, S. (2016). Immune Sensing of Lipopolysaccharide in Plants and Animals: Same but Different. *PLoS pathogens* **12**, e1005596.

Reeves, P. (1965). The Adsorption And Kinetics Of Killing By Colicin Ca42-E2. *Aust J Exp Biol Med Sci* **43**, 191-200.

Ruhe, Z.C., Low, D.A., and Hayes, C.S. (2020). Polymorphic Toxins and Their Immunity Proteins: Diversity, Evolution, and Mechanisms of Delivery. *Annual review of microbiology* **74**, 497-520.

Sanchez-Garcia, R., Gomez-Blanco, J., Cuervo, A., Carazo, J., Sorzano, C., and Vargas, J. (2020). DeepEMhacer: a deep learning solution for cryo-EM volume post-processing. *bioRxiv*, 2020.2006.2012.148296.

Scheres, S.H.W. (2012a). A Bayesian View on Cryo-EM Structure Determination. *Journal of molecular biology* **415**, 406-418.

Scheres, S.H.W. (2012b). RELION: Implementation of a Bayesian approach to cryo-EM structure determination. *Journal of Structural Biology* **180**, 519-530.

Schneider, C.A., Rasband, W.S., and Eliceiri, K.W. (2012). NIH Image to ImageJ: 25 years of image analysis. *Nature Methods* **9**, 671-675.

Soelaiman, S., Jakes, K., Wu, N., Li, C.M., and Shoham, M. (2001). Crystal structure of colicin E3: Implications for cell entry and ribosome inactivation. *Molecular Cell* **8**, 1053-1062.

- 1148 Szczepaniak, J., Holmes, P., Rajasekar, K., Kaminska, R., Samsudin, F., Inns, P.G.,  
1149 Rassam, P., Khalid, S., Murray, S.M., Redfield, C., *et al.* (2020). The lipoprotein Pal  
1150 stabilises the bacterial outer membrane during constriction by a mobilisation-and-capture  
1151 mechanism. *Nature communications* 11, 1305.
- 1152
- 1153 Vankemmelbeke, M., Healy, B., Moore, G.R., Kleanthous, C., Penfold, C.N., and James, R.  
1154 (2005). Rapid detection of colicin E9-induced DNA damage using *Escherichia coli* cells  
1155 carrying SOS promoter-lux fusions. *Journal of bacteriology* 187, 4900-4907.
- 1156
- 1157 Vankemmelbeke, M., Housden, N.G., James, R., Kleanthous, C., and Penfold, C.N. (2013).  
1158 Immunity protein release from a cell-bound nuclease colicin complex requires global  
1159 conformational rearrangement. *MicrobiologyOpen* 2, 853-861.
- 1160
- 1161 Vergalli, J., Bodrenko, I.V., Masi, M., Moynie, L., Acosta-Gutierrez, S., Naismith, J.H., Davin-  
1162 Regli, A., Ceccarelli, M., van den Berg, B., Winterhalter, M., *et al.* (2020). Porins and small-  
1163 molecule translocation across the outer membrane of Gram-negative bacteria. *Nature*  
1164 *reviews. Microbiology* 18, 164-176.
- 1165
- 1166 Walker, D., Mosbahi, K., Vankemmelbeke, M., James, R., and Kleanthous, C. (2007). The  
1167 role of electrostatics in colicin nuclease domain translocation into bacterial cells. *The Journal*  
1168 *of biological chemistry* 282, 31389-31397.
- 1169
- 1170 Wang, F., Liu, Y., Yu, Z., Li, S., Feng, S., Cheng, Y., and Agard, D.A. (2020). General and  
1171 robust covalently linked graphene oxide affinity grids for high-resolution cryo-EM.  
1172 *Proceedings of the National Academy of Sciences* 117, 24269-24273.
- 1173
- 1174 White, P., Joshi, A., Rassam, P., Housden, N.G., Kaminska, R., Goult, J.D., Redfield, C.,  
1175 McCaughey, L.C., Walker, D., Mohammed, S., *et al.* (2017). Exploitation of an iron  
1176 transporter for bacterial protein antibiotic import. *Proceedings of the National Academy of*  
1177 *Sciences of the United States of America* 114, 12051-12056.
- 1178
- 1179 Whitfield, C., and Trent, M.S. (2014). Biosynthesis and export of bacterial  
1180 lipopolysaccharides. *Annual review of biochemistry* 83, 99-128.
- 1181
- 1182 Yanisch-Perron, C., Vieira, J., and Messing, J. (1985). Improved M13 phage cloning vectors  
1183 and host strains: nucleotide sequences of the M13mp18 and pUC19 vectors. *Gene* 33, 103-  
1184 119.
- 1185
- 1186 Zhang, K. (2016). Gctf: Real-time CTF determination and correction. *Journal of Structural*  
1187 *Biology* 193, 1-12.
- 1188
- 1189 Zheng, S.Q., Palovcak, E., Armache, J.-P., Verba, K.A., Cheng, Y., and Agard, D.A. (2017).  
1190 MotionCor2: anisotropic correction of beam-induced motion for improved cryo-electron  
1191 microscopy. *Nature Methods* 14, 331-332.
- 1192
- 1193 Zivanov, J., Nakane, T., Forsberg, B.O., Kimanius, D., Hagen, W.J.H., Lindahl, E., and  
1194 Scheres, S.H.W. (2018). New tools for automated high-resolution cryo-EM structure  
1195 determination in RELION-3. *eLife* 7, e42166.
- 1196
- 1197 Zivanov, J., Nakane, T., and Scheres, S.H.W. (2020). Estimation of high-order aberrations  
1198 and anisotropic magnification from cryo-EM data sets in RELION-3.1. *IUCrJ* 7, 253-267.
- 1199

# Figures

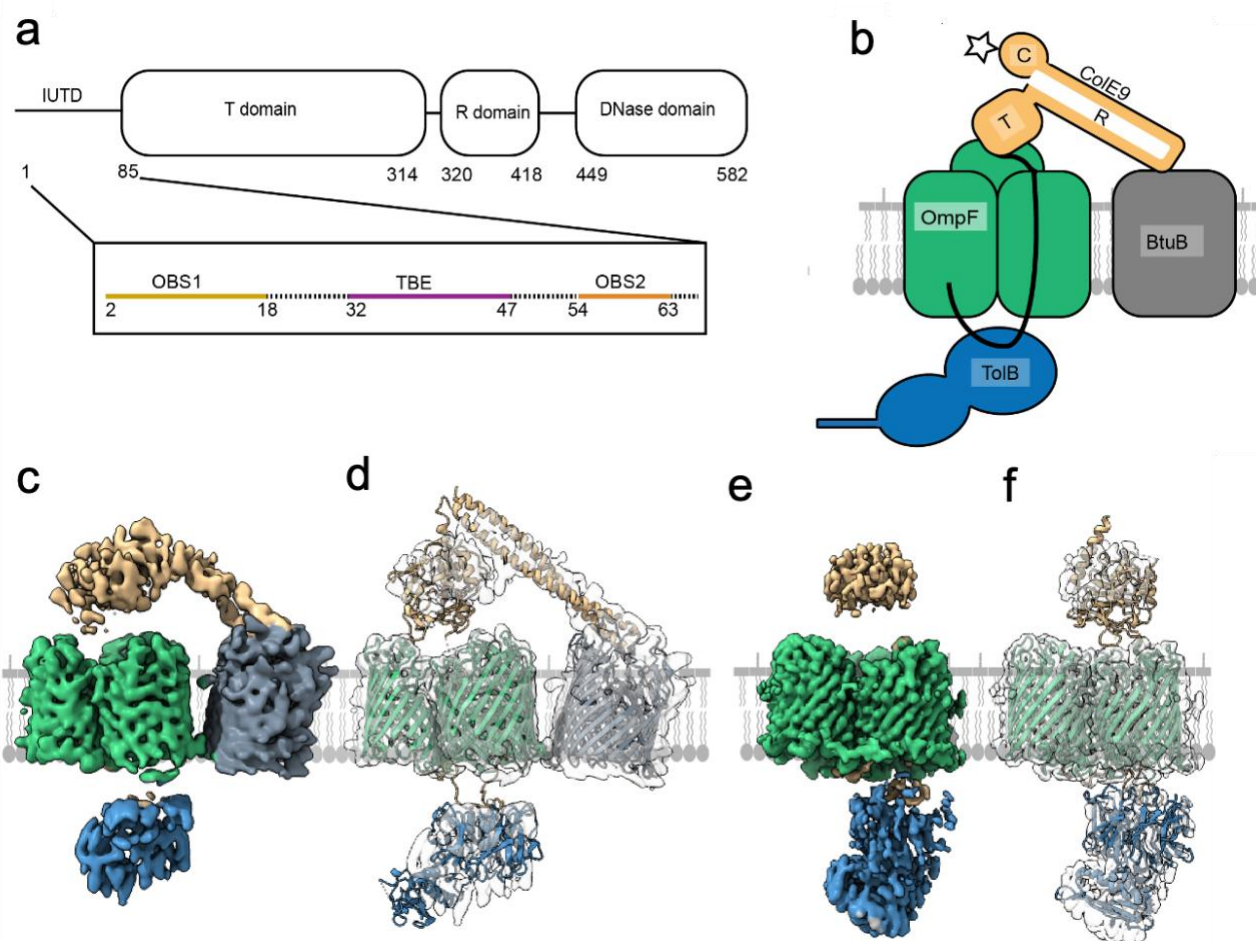


**Figure 1. Cryo-EM structures of the ColE9 outer membrane translocon.** **a**, Schematic of the ColE9 sequence showing its constituent domains: an intrinsically unstructured translocation domain (IUTD) at the N-terminus is followed by three structured domains involved in translocation (T), receptor (R) binding and cytotoxicity (C). The IUTD houses three linear protein-protein interaction epitopes, two OmpF binding sites (OBS1, OBS2) flank a TolB-binding epitope (TBE). Residue numbers denote position in ColE9 sequence. **b**, Cartoon of the ColE9 OM translocon. ColE9 (orange) exploits the vitamin B<sub>12</sub> transporter BtuB (grey) as its extracellular receptor and the porin OmpF (green) for threading its N-terminal IUTD (solid black line) through to the periplasm where it captures TolB (blue). Star, represents the site on the ColE9 DNase domain (K469C) where fluorophores were covalently attached throughout this study. **c**, Cryo-EM map of the fully assembled ColE9 translocon, with local resolution range 4.5-16 Å. Component proteins are coloured as in

1215 panel b. The structure shows extracellular ColE9 creating a protein bridge between the two  
1216 OMPs, BtuB and OmpF. The  $\beta$ -barrel of BtuB is tilted by 35° relative to that of OmpF. TolB  
1217 is located on the periplasmic side of OmpF, with no associations to BtuB. ColE9 and TolB  
1218 regions of the map have weaker density than those of the  $\beta$ -barrels. **d**, Model of the intact  
1219 ColE9 translocon generated after docking and rigid-body refinement of individual structures  
1220 of ColE9 residues 85-580 (PDB ID 5EW5), OmpF (3K19), BtuB (PDB ID 2YSU), and TolB  
1221 (PDB ID 4JML). **e**, Cryo-EM map of the partial ColE9 translocon with an average resolution  
1222 of 3.7 Å, which has density consistent with OmpF, TolB, and ColE9 residues 3-314. Map is  
1223 coloured based on component parts shown in panel b. TolB is much better resolved here  
1224 than in the full translocon map in panel c, although ColE9 density is weaker. ColE9 and  
1225 TolB density aligns on the extracellular and periplasmic side of OmpF, respectively. **f**, The  
1226 refined structure of the partial translocon, generated by docking and refinement of ColE9  
1227 residues 85-580 (PDB ID 5EW5), OmpF (PDB ID 3K19), and TolB-ColE9 TBE (PDB ID  
1228 4JML). ColE9 residues 3-75 were built *de novo*.

1229

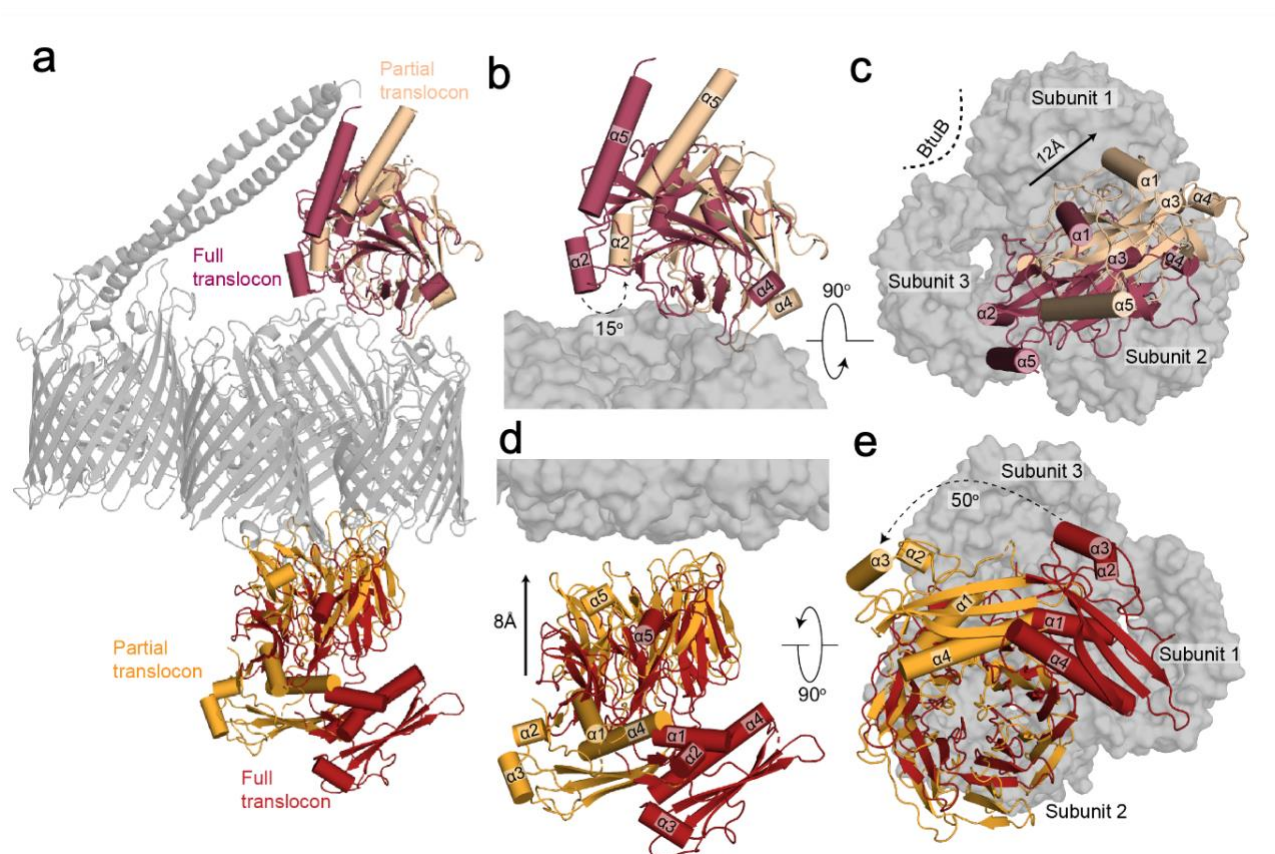


**Figure 2. Large-scale structural rearrangements accompany the loss of BtuB from the ColE9 translocon.** **a**, Superposition of the complete and partial ColE9 translocon structures (grey) aligned on OmpF. TolB in red and orange denote the full and partial translocons, respectively, ColE9 T-domain is presented in crimson and pale orange for the full and partial translocons, respectively. **b**, Sideview comparison showing the relative positions of the ColE9 T-domain (residues 85-316) in the two structures and highlighting the 15° rotation that occurs transitioning from the full (crimson) to the partial (pale orange) translocon. **c**, Extracellular view of the ColE9 T-domain position, with the OmpF trimer shown in the background. The loss of BtuB from the translocon complex elicits a 12 Å movement along the axis of rotation (black arrow) that results in repositioning of the T-domain from a central location (crimson) to above subunit two of OmpF (pale orange). **d**, TolB undergoes both rotation and translation when transitioning from the full (red) to the partial translocon (orange). The C-terminal β-propeller domain of TolB, which binds the ColE9 TBE, moves toward OmpF in the OM by ~8 Å along the rotation axis. **e**, View along

1245 the rotation axis from the periplasmic side of OmpF (*grey surface*) highlighting the 50°  
1246 rotation that TolB undergoes upon loss of BtuB from the translocon complex.  
1247

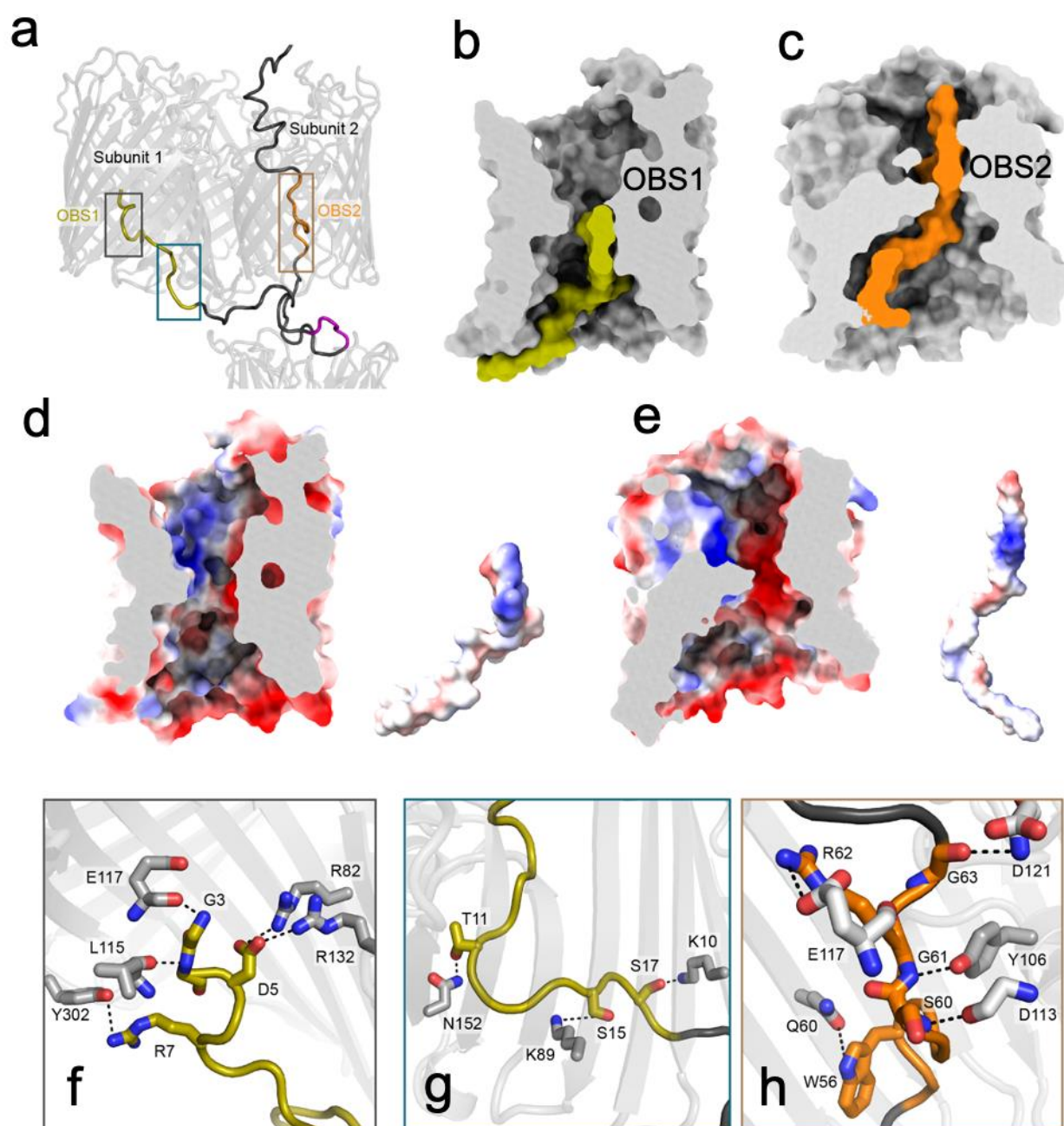


**Figure 3. Distinct modes of ColE9 OBS1 and OBS2 recognition within the pores of OmpF enable threading and the tethered presentation of the TBE to the periplasm.** **a**, ColE9 residues 3-75 of the IUTD in the partial translocon structure pass through OmpF subunit 2 and then back up into subunit 1. As a result, OBS1 (*gold*) docks within subunit 1 and OBS2 (*orange*) within subunit 2. The ColE9 TBE motif (*pink*) interacts with TolB is positioned below subunit 2, above which the ColE9 T-domain is located. **b**, Surface representation of OmpF subunit 1 (*grey*) and ColE9 residues 3-24 (*gold*) containing OBS1 sequence. ColE9 OBS1 binds the inner vestibule of OmpF subunit 1 such that it runs along

1257 the edge of the vestibule, stopping at the eyelet. **c**, ColE9 residues 45-70 (*orange*)  
1258 encompassing OBS2, traverse the pore of OmpF subunit 2 (*grey*). After passing through  
1259 the eyelet, OBS2 tracks more centrally into the inner vestibule unlike in panel c where  
1260 residues 3-24 trail the side of the pore. **d**, OmpF subunit 1 displayed as an electrostatic  
1261 surface (same cut-through as in b), revealing a patch of negative charge located on the  
1262 extracellular side of the eyelet that interacts with OBS1, which is contained within the  
1263 sequence (residues 3-24) also shown as an electrostatic surface adjacent to the subunit. **e**,  
1264 OmpF subunit 2 displayed as an electrostatic surface (same cut-through as in c), with  
1265 residues 45-70 also shown as an electrostatic surface adjacent to the subunit. Projecting  
1266 out of the page in the OBS2 sequence is a positively charged region flanked by negative  
1267 charges. **f**, A zoom-in of grey box in panel a highlighting hydrogen bonding network between  
1268 residues 3-7 of OBS1 (*gold sticks*) and nearby residues within OmpF subunit 1 (*grey sticks*).  
1269 **g**, OBS1 residues 11-17 (*gold sticks*) also interact with the base of OmpF subunit 1 (*grey*  
1270 *sticks*) in the periplasm. Region is a zoom-in of blue box in panel a. **h**, OmpF subunit 2  
1271 residues (*grey sticks*) form a hydrogen bond network with the backbone of residues of ColE9  
1272 OBS2. Region is a zoom-in of brown box in panel a. All electrostatic surfaces shown in  
1273 panels d and e were calculated using the APBS plugin within Pymol.

1274

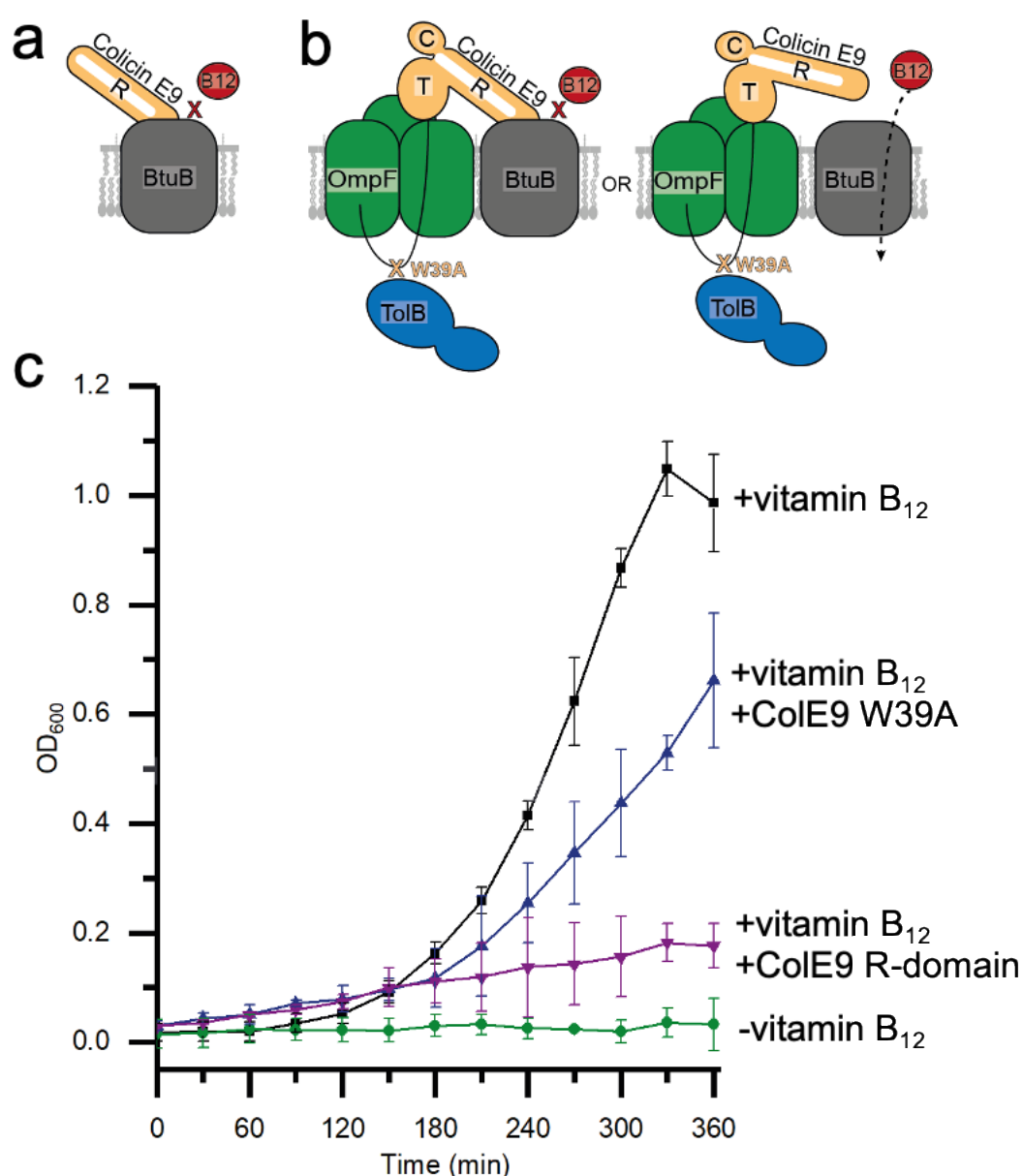


**Figure 4. ColE9 threading through the subunits of OmpF disengages the toxin from its outer membrane receptor, BtuB.** **a**, Cartoon depicting the basis for the control where the isolated R-domain of ColE9 (residues 348-418, orange), which binds BtuB (grey) with higher affinity than vitamin B<sub>12</sub> (red), impairs growth of *E. coli* 113/3, a B<sub>12</sub>-dependent strain (Penfold et al., 2000). **b**, Cartoon schematic of the two possible translocon outcomes for ColE9 W39A and their implications on vitamin B<sub>12</sub> import in *E. coli* 113/3. The W39A mutation within the TBE of ColE9 (orange) impairs TolB (blue) binding thereby uncoupling the OM components of the translocon from the energized TolQ-TolR-TolA complex in the

1284 inner membrane. If threading of the ColE9 IUTD through OmpF (*green*) has no impact on  
1285 ColE9 binding to BtuB (*grey*) then vitamin B<sub>12</sub> (*red*) cannot enter cells to support growth. In  
1286 contrast, if OmpF threading disengages ColE9 from BtuB then vitamin B<sub>12</sub> can enter cells to  
1287 support growth. **c**, Growth curves for *E. coli* 113/3 in defined media and in the presence or  
1288 absence of B<sub>12</sub> (*black* and *green*, respectively). When challenged with 40 nM isolated R-  
1289 domain (*purple*), cell growth was largely impaired whereas growth in the presence of 40 nM  
1290 ColE9 W39A (*blue*) approached that of the no colicin control, consistent with OmpF  
1291 threading causing the disengagement of ColE9 from BtuB.  
1292

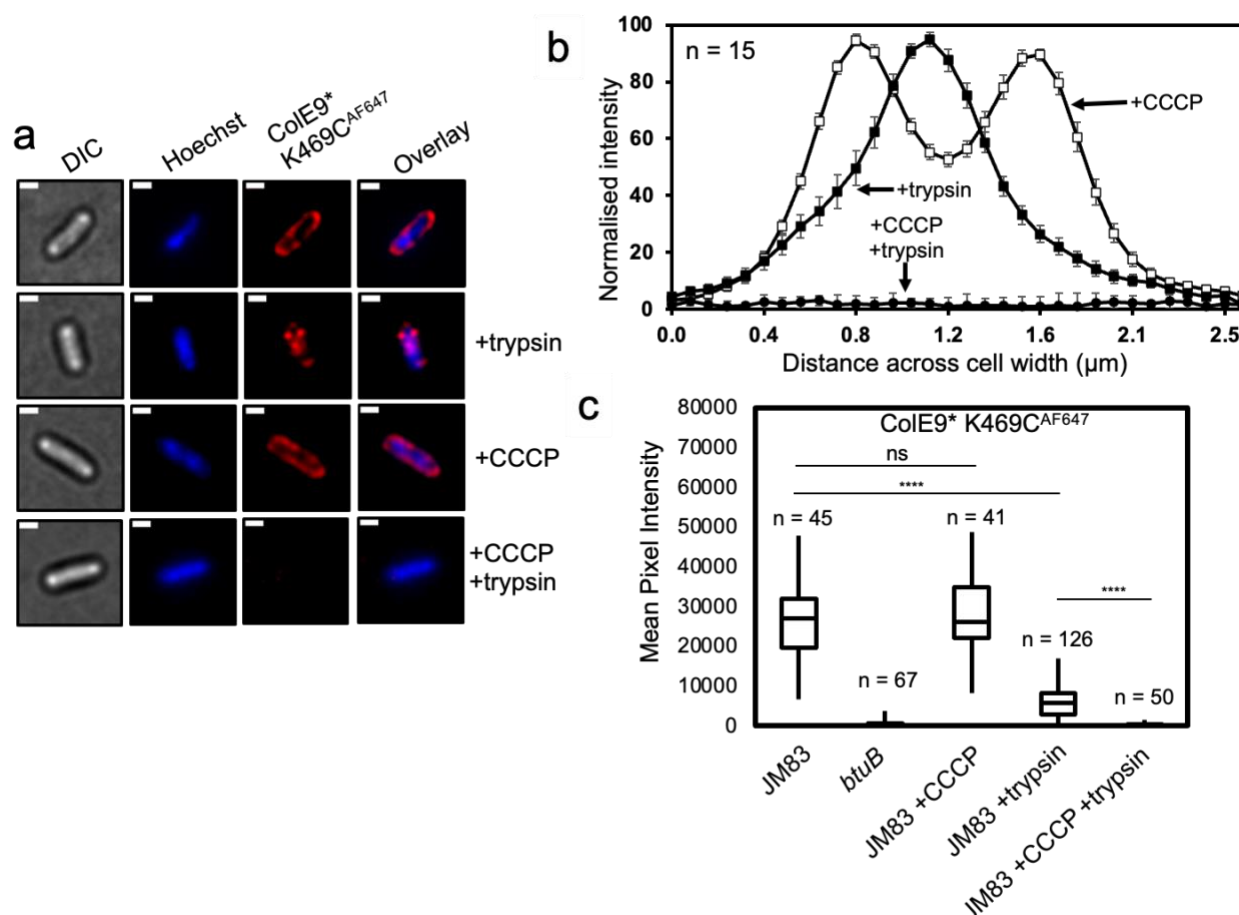


**Figure 5. ColE9\* K469C<sup>AF647</sup> translocation across the outer membrane is PMF dependent.** ColE9\*, denotes ColE9 H551A, an active site mutation that inactivates the toxin. **a**, Widefield fluorescence microscopy images of *E. coli* JM83 cells labelled with ColE9\* K469C<sup>AF647</sup> (1.5  $\mu$ M) and Hoechst DNA stain (20  $\mu$ M) for 30 min at 37  $^{\circ}$ C with or without trypsin treatment with or without prior treatment with CCCP. Each panel show the same cell in DIC (grey), Hoechst DNA stain (blue) and ColE9\* K469C<sup>AF647</sup> fluorescence (red). Overlays of Hoechst and ColE9\* K469C<sup>AF647</sup> fluorescence are also shown. ColE9\* K469C<sup>AF647</sup> remains bound to the OM in the presence of CCCP but this signal is lost on treatment with trypsin. Trypsin treatment in the absence of CCCP yields some cell-associated ColE9\* K469C<sup>AF647</sup> fluorescence that likely represents internalised molecules. Scale bar, 1  $\mu$ m. **b**, Fluorescence intensity across *E. coli* JM83 cell widths for each condition measured in ImageJ, n = 15 cells per condition. CCCP-treated cells showed peripheral ColE9\* K469C<sup>AF647</sup> fluorescence consistent with the colicin being bound at the OM. Trypsin

1307 treatment of cells in the absence of CCCP results in loss of this peripheral fluorescence but  
 1308 the presence of mid-cell signal consistent with internalisation. Treatment with CCCP and  
 1309 trypsin removed all ColE9\* K469C<sup>AF647</sup> fluorescence from cells, as in a. Mann-Whitney U-  
 1310 test performed between the +CCCP and the +trypsin data sets between cell distances of  
 1311 0.8-1.6  $\mu\text{m}$ , gave a value of  $U = 0.04$ , showing that there is a significant difference between  
 1312 these two data sets. Error bars represent % SEM. **c**, Box and whisker plots showing mean  
 1313 pixel intensities for ColE9\* K469C<sup>AF647</sup> fluorescence per cell measured for the indicated cells  
 1314 and condition used, whiskers represent minimum and maximum mean pixel intensity, box  
 1315 shows 1<sup>st</sup> and 3<sup>rd</sup> quartile with the median shown as a line. From left-to-right: *E. coli* JM83  
 1316 cells; *E. coli* *btuB* deletion strain showing loss of all ColE9\* K469C<sup>AF647</sup> cell-associated  
 1317 fluorescence; *E. coli* JM83 cells in the presence of CCCP; *E. coli* JM83 cells following trypsin  
 1318 treatment showing significant ColE9\* K469C<sup>AF647</sup> fluorescence remains associated with  
 1319 cells indicative of import; *E. coli* JM83 cells treated with CCCP and trypsin showing the  
 1320 complete loss of internalised ColE9\* K469C<sup>AF647</sup> fluorescence. *n*, number of cells used,  
 1321 typically from 2-4 biological replicates. \*\*\*\*, indicates a P value below 0.0001 in a one-way  
 1322 ANOVA multiple comparisons Kruskal-Wallis test, ns indicates no significant difference.

1323

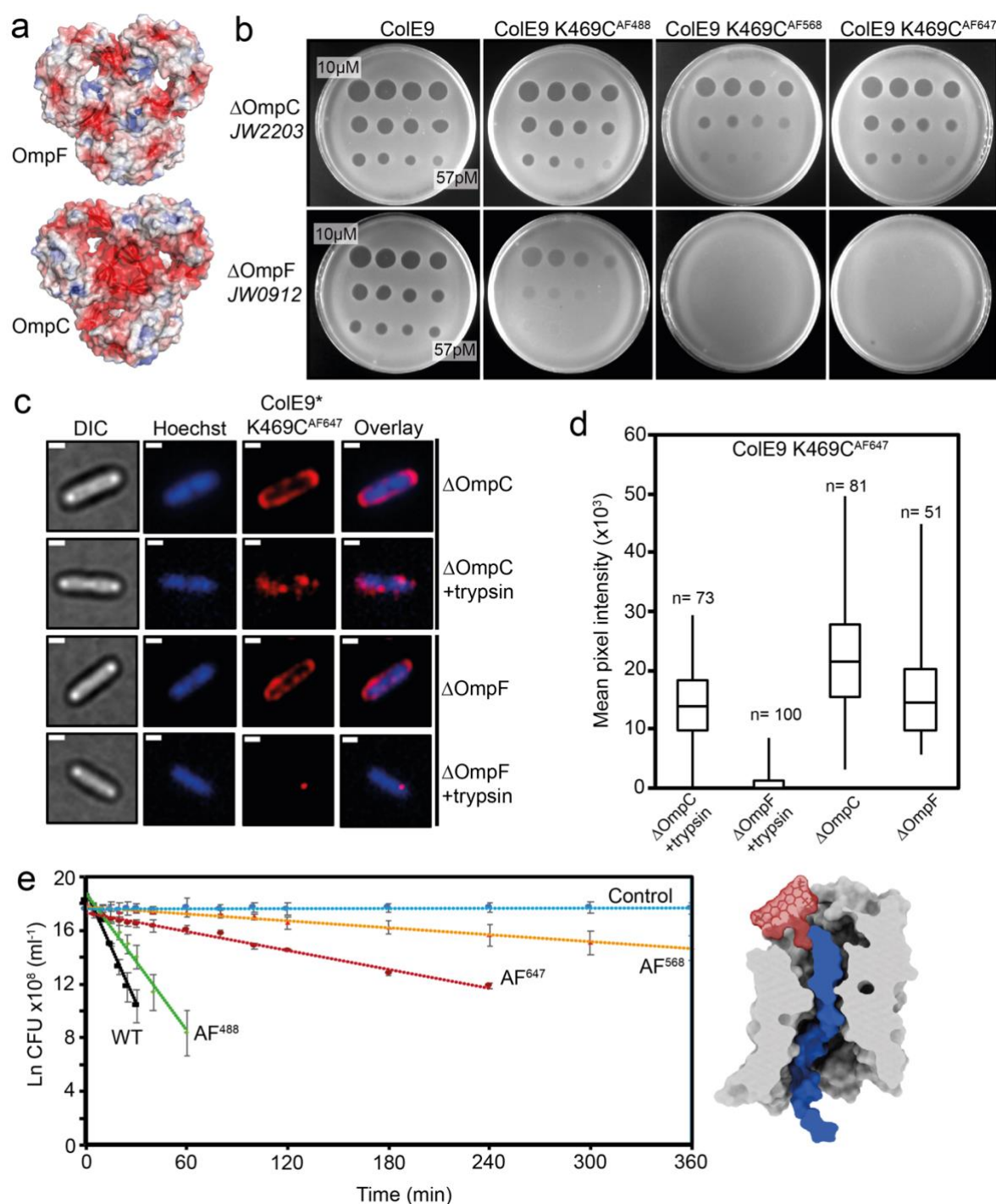
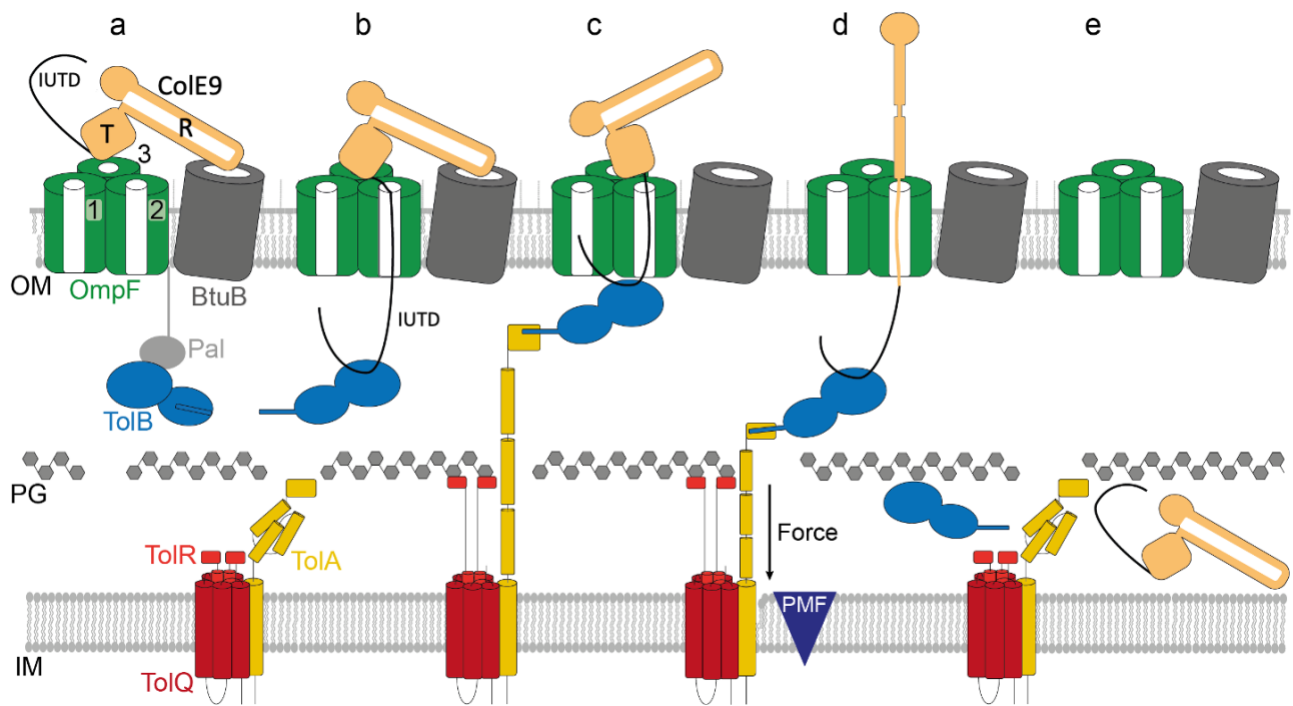


**Figure 6. Labelling ColE9 with fluorophores impedes its translocation through the pores of OmpC.** **a**, Cut-through molecular surface images showing the distribution of charged residues (acidic, red; basic, blue) at the eyelets of trimeric OmpF (PDB ID 3K19) and OmpC (PDB ID 2J1N). The eyelet of OmpC is significantly more electronegative than that of OmpF. Electrostatic surfaces were calculated using the APBS plugin within Pymol. **b**, Overnight plate assays comparing the cytotoxic activity of wild-type ColE9 with ColE9

1331 K469C labelled with AF488, AF568 or AF647 against a lawn of *E. coli* with either OmpF  
1332 (JW2203) or OmpC (JW0912) in the outer membrane. Each plate was spotted with a serial  
1333 dilution of the colicin (10  $\mu$ M - 57 pM). Wild-type ColE9 was equally active against both  
1334  $\Delta$ OmpF and  $\Delta$ OmpC cells, whereas labelling ColE9 K469C with fluorophores reduced  
1335 (AF488) or abolished (AF568, AF647) colicin activity in  $\Delta$ OmpF cells, whilst activity against  
1336  $\Delta$ OmpC cells remained comparable to that of wild-type ColE9. **c**, Widefield fluorescence  
1337 microscopy images of *E. coli* JW2203 (*ompF*-expressing) and JW0912 (*ompC*-expressing)  
1338 cells labelled with ColE9\* K469C<sup>AF647</sup> (1.5  $\mu$ M) and Hoechst stain (20  $\mu$ M) for 30 min at 37 °C  
1339 with or without trypsin treatment. Each panel shows the same cell in, DIC (*grey*), Hoechst  
1340 DNA stain (*blue*) and fluorescence of ColE9\* K469C<sup>AF647</sup> (*red*). Overlays of Hoechst and  
1341 ColE9\* K469C<sup>AF647</sup> fluorescence are also shown. Data show that following trypsin-treatment  
1342 significant ColE9\* K469C<sup>AF647</sup> fluorescence remains associated with *ompF*-expressing *E.*  
1343 *coli* whereas little or no fluorescence remains associated with *ompC*-expressing *E. coli*.  
1344 Scale bar, 1  $\mu$ m. **d**, Box and whisker plots of *E. coli* JW2203 and *E. coli* JW0912 cells  
1345 labelled with ColE9\* K469C<sup>AF647</sup> with and without trypsin treatment: whiskers represent  
1346 minimum and maximum mean pixel intensity, box shows 1<sup>st</sup> and 3<sup>rd</sup> quartile with the median  
1347 shown as a line. Microscopy data were collected as in c. The mean pixel intensity of ColE9\*  
1348 K469C<sup>AF647</sup> per cell was measured for each cell condition. *n*, number of cells, typically from  
1349 3 or 4 biological replicates. Data show that ColE9\* K469C<sup>AF647</sup> translocates across the OM  
1350 through OmpF and that this is significantly impeded when *E. coli* has OmpC in the outer  
1351 membrane. **e**, Shows first-order cell death kinetics for wild-type ColE9 or ColE9 K469C  
1352 labelled with different AF dyes (AF488, AF568, AF647) against *E. coli* JW2203 *ompF*-  
1353 expressing cells. Cultures were incubated with 80 nM toxin at pH 7.5 and 37 °C and at  
1354 various time points the reaction stopped using trypsin at 37 °C for 30 min, cells plated out  
1355 and CFUs recorded. All time courses were conducted in the presence of chloramphenicol  
1356 (20  $\mu$ g/ml) to reversibly block cell division, which would otherwise compete with cell-killing.

Control data shown are for cells with no ColE9 added but where growth was inhibited by the presence of chloramphenicol. Cell-killing half-lives, obtained from the fitted first-order plots shown (error bars from two biological replicates), were as follows: wild-type ColE9, 2.5 min; ColE9 K469C<sup>AF488</sup>, 4.1 min; ColE9 K469C<sup>AF647</sup>, 29.6 min; ColE9 K469C<sup>AF568</sup>, 78.8 min. The data show that the chemical nature of the fluorophore in the C-terminal DNase domain of ColE9 has a dramatic effect on the cell-killing kinetics of the colicin. Schematic surface representation in which AF568 (model Generated in coot), the fluorophore with the biggest impact on OmpF-mediated killing, has been manually grafted onto the structure of ColE9 OBS2 bound within subunit 2 of OmpF. The slow cell-death kinetics of ColE9 K469C<sup>AF568</sup> likely reflects the time taken to pass this bulky molecule through the narrow eyelet of the porin.

56



1369

1370

1371

1372

1373

1374

1375

1376

1377

1378

1379

1380

1381

1382

1383

1384

1385

1386

1387

1388

1389

1390

**Figure 7. Model of ColE9 translocon assembly and energised OM transport** (see text for details). **a**, ColE9 R-domain binds BtuB with high affinity, positioning the T-domain and IUTD above a neighbouring OmpF trimer. **b**, The ColE9 IUTD translocates through subunit 2 of OmpF to deposit the TBE in the periplasm and capture TolB at the expense of the OM lipoprotein Pal. The TBE allosterically promotes displacement of TolB's N-terminus which constitutes the TolA binding site. We propose this complex equates to the full translocon cryo-EM structure. **c**, ColE9 OBS1 binds subunit 1 of OmpF from the periplasm. Threading through two of OmpFs three subunits drives dissociation of the ColE9 R-domain-BtuB complex and reorients the T-domain above subunit 2 below which TolB is positioned in the periplasm. The docking of OBS1 also results in TolB moving closer to the opening of subunit 2. This complex, which we propose equates to the partial translocon cryo-EM structure, is now primed for contact with TolA in the inner membrane. TolA extension through the periplasm is coupled to the PMF via its stator proteins, TolQ and TolR. **d**, Retraction of TolA (the molecular mechanism of which remains to be established) provides the driving force for pulling ColE9 bound to TolB into the periplasm through subunit 2 of OmpF, accompanied by unfolding of its constituent domains. It is at this point the immunity protein Im9 (not shown) would be displaced at the cell surface. **e**, The TolA-TolB complex is thought to retract through the cell wall, which would bring ColE9 close to the cytoplasmic membrane. The toxin likely refolds prior to transport across the cytoplasmic membrane, which involves the AAA<sup>+</sup>ATPase/protease FtsH (not shown) (Walker et al., 2007).